

See discussions, stats, and author profiles for this publication at: <https://www.researchgate.net/publication/259495752>

Numerical Modeling of Laminar Flames with Detailed Kinetics Based on the Operator-Splitting Method

ARTICLE in ENERGY & FUELS · DECEMBER 2013

Impact Factor: 2.79 · DOI: 10.1021/ef4016334

CITATIONS

6

READS

77

4 AUTHORS, INCLUDING:



[Alberto Cuoci](#)

Politecnico di Milano

91 PUBLICATIONS 1,001 CITATIONS

[SEE PROFILE](#)



[Alessio Frassoldati](#)

Politecnico di Milano

106 PUBLICATIONS 1,845 CITATIONS

[SEE PROFILE](#)



[Eliseo Ranzi](#)

Politecnico di Milano

225 PUBLICATIONS 4,783 CITATIONS

[SEE PROFILE](#)

Numerical Modeling of Laminar Flames with Detailed Kinetics Based on the Operator-Splitting Method

Alberto Cuoci,* Alessio Frassoldati, Tiziano Faravelli, and Eliseo Ranzi

Department of Chemistry, Materials, and Chemical Engineering, Politecnico di Milano, P.zza Leonardo da Vinci 32, 20133 Milano, Italy

S Supporting Information

ABSTRACT: In this work, we applied and analyzed a new computational code, called `laminarSMOKE`, for the numerical simulation of laminar flames in complex, multidimensional geometries with detailed kinetic mechanisms. The code, built on top of the open-source `OpenFOAM` platform, solves the usual transport equations of mass, momentum, energy, and species for reacting flows on both structured and unstructured meshes. The operator-splitting technique is adopted in order to effectively face the reacting, stiff processes associated with detailed kinetics. The proposed algorithm was used to simulate different combustion systems with different degrees of complexity under both steady-state and transient conditions. In particular, simulations of 1D and 2D laminar premixed flames, 2D counter-flow diffusion flames, and coflow flames (purely diffusive and partially premixed) were successfully performed, demonstrating that the proposed tool is a robust, accurate solution method for laminar flames. In particular, the simulations of coflow, laminar flames with very detailed kinetic mechanisms (~200 species) resulted in very good agreement with published experimental data. Despite its generality (i.e., the ability to manage arbitrarily complex multidimensional geometries), the `laminarSMOKE` code showed satisfactory scalability up to 96 processors. More importantly, as demonstrated by Tosatto et al. [*Combustion Theory and Modeling* 2011, 15 (4), 455–486], it was observed that the parallel efficiency increased with the number of species in the kinetic scheme adopted. This makes the proposed code an ideal framework for the numerical simulation of combustion systems with very detailed kinetic schemes. In contrast to most of the existing codes for the simulation of reacting systems with detailed kinetics, the `laminarSMOKE` code is freely distributed on the web (<http://www.opensmoke.polimi.it/>).

1. INTRODUCTION

Numerical modeling is becoming an important, powerful, and effective tool for the design of advanced and efficient combustion systems, especially because of the recent advances in computational fluid dynamics (CFD), numerical methods for reacting flows, and advances in high-performance-computing hardware.¹ The increasing demand for computational tools that are able to characterize complex combustion systems can be also explained by the increasingly stringent legislation imposed by governments worldwide about the emissions of pollutant species, such as nitrogen oxides (NO_x), polycyclic aromatic hydrocarbons (PAHs), soot, etc. This has been making the design process of combustion devices much more challenging. Numerical models that can characterize a combustion system in a predictive way, not only in terms of temperature and flow fields but also in terms of the formation of pollutant species, are required to help in the design of gas turbines, industrial furnaces, internal combustion engines, industrial and domestic burners, etc.

Even though most practical combustion systems involve turbulent combustion, the numerical simulation of flames under laminar conditions has received extensive attention in the last 20 years. Indeed, laminar conditions are the ideal framework to study the mechanisms leading to the formation of pollutant species without introducing the additional difficulties associated with the modeling of the complex interactions between turbulence and kinetics. In other words, this provides the possibility to focus the attention on the chemical aspects, which

are of paramount importance when the objective is the prediction of pollutants and particulate emissions. Pollutant species are controlled by the details of the fuel–air mixing, and usually the correct prediction of their formation requires the adoption of very detailed kinetic mechanisms involving hundreds of species and thousands of reactions. This means that the numerical modeling of combustion systems with an accurate description of pollutants is a very CPU-intensive computational problem, since a large number of transport equations must be solved. In addition, the transport equations for species are usually very nonlinear because of the source terms (formation and consumption due to chemical reactions), which involve the exponential of the temperature through the Arrhenius law.² The overall problem is highly stiff because the spectrum of characteristic times characterizing the evolution of different species is very large. The discretization in space has to be sufficiently fine to properly describe the high gradients of density, temperature and composition close to the flame front. Therefore, the numerical modeling of laminar flames in 2D and 3D geometries with realistic kinetic schemes can be considered a challenging problem and poses strong requests on the computational resources. The resulting memory requirements and the computational efforts (i.e., the CPU time) are significant and often prohibitive.

Received: May 31, 2013

Revised: October 21, 2013

Published: October 21, 2013

The main efforts developed in the last years to model multidimensional flames are summarized in the following paragraphs. The attention is focused on the numerical models that are able to manage detailed kinetic schemes, especially under laminar conditions.

A computationally low-cost numerical platform was developed by Ern et al.³ to solve reacting flows at low Mach number using a velocity–vorticity formulation. They adopted a fully coupled strategy implemented through a domain decomposition technique, with satisfactory performances on multiprocessor architectures. Several physical submodels (mainly soot formation and radiative heat transfer⁴), together with numerical aspects,^{5–7} were improved over the years. In particular, the same strategy was also extended to 3D steady compressible flows.⁸ However, as reported by the same authors, one of the main disadvantages of the velocity–vorticity formulation is represented by the difficulty in treating the boundary conditions with a sufficiently high degree of accuracy.⁷

More recently, Tosatto et al.⁹ extended the work of Ern et al.³ by deeply investigating the use of fully implicit methods on distributed memory for the solution of 2D laminar axisymmetric coflow diffusion flames. In particular, in ref 9 three different parallel implementations of Newton's method were implemented and tested, and different grid decomposition techniques were analyzed. The parallel code was then effectively applied to solve a coflow diffusion flame (fed with a mixture of prevaporized JP8 and air) with a kinetic mechanism involving 222 species. Good parallelization efficiencies of about 80% and speedups of 20–100 were observed.

Knio et al.¹⁰ developed a stiff operator split projection scheme for the simulation of reacting flows with detailed kinetic mechanisms. The proposed numerical methodology was applied to study the interaction between a counter-rotating vortex pair and a premixed methane/air flame using the GRI 1.2 mechanism,¹¹ with excellent results in terms of accuracy and stability.

Consul et al.¹² developed a parallel algorithm for the numerical simulation of multidimensional laminar flames that is able to work efficiently with loosely coupled computers. The numerical algorithm is based on the operator-splitting approach, and great attention is devoted to the treatment of the stiffness of the chemical step (which is solved using the modified damped Newton's method). Good parallel performances (efficiencies of ~70%) were achieved through the domain decomposition method, but only on a limited number of processors.

Becker et al.¹³ simulated several laminar flames using a detailed kinetic scheme by adopting finite elements in order to refine the mesh automatically and adaptively on the basis of an estimation of the discretization error.

A numerical platform for modeling laminar coflow flames was developed by D'Anna et al.¹⁴ and applied to study the growth of hydrocarbons. The transport equations are solved using a first-order finite-volume advective scheme. The linearized equations are solved by adopting the alternating-direction implicit (ADI) scheme and a tridiagonal matrix algorithm (TDMA).

Liu et al.¹⁵ and Guo et al.¹⁶ proposed a solver for structured meshes based on the finite-volume method. The SIMPLE technique was adopted to deal with pressure–velocity coupling.¹⁷ The equations of mass, momentum, and energy

are solved using a segregated approach based on the TDMA. A multigrid method is employed to solve the equations of single species. One of the major drawbacks is that this technique cannot be applied for time-accurate studies, as reported by the same authors.

Katta and co-workers developed a time-dependent, axisymmetric mathematical model called UNICORN^{18,19} to simulate unsteady jet-diffusion flames. The code works on a staggered-grid system and solves the equations of continuity, momentum, enthalpy, and species. In order to accurately trace the large gradients in flow variables close to the flame front, a clustered mesh system is employed. Detailed kinetic mechanisms consisting of dozens of species can be used by UNICORN to investigate heavy hydrocarbon fuels. An implicit QUICKEST scheme²⁰ is applied to discretize the momentum equations, while the species and energy equations are discretized using a hybrid scheme of upwind and central differencing. At each time step, the pressure field is accurately calculated by solving all of the pressure Poisson equations simultaneously and using the lower and upper tridiagonal (LU) matrix-decomposition technique.

Burman et al.²¹ proposed a code based on the finite element method that can solve the equations governing laminar reacting flows on unstructured, triangular meshes that are adaptively refined using an a posteriori error estimate derived from the dual weighted residual method. The proposed approach was successfully applied to simulate a Bunsen flame using a hydrogen/air kinetic scheme.

A parallel algorithm based on a fractional step method was proposed by Day and Bell²² and Bell et al.²³ to solve both steady-state and unsteady reacting flows under the low-Mach-number limit. Complex geometries can be effectively simulated thanks to the possibility of exploiting adaptive mesh refinement (AMR) to solve the equations. Satisfactory parallel performances were observed, with efficiencies around 70–80%.

Gao et al.¹ proposed a highly parallelized AMR scheme for obtaining steady-state solutions of 3D non-premixed combustion flows. The system of PDEs governing the flows of reactive thermally perfect gaseous mixtures uses a fully coupled finite-volume formulation on a body-fitted multiblock hexahedral mesh. The combination of a block-based AMR strategy, hierarchical tree data structure, and parallel implementation results in a highly scalable computational tool. However, only a global mechanism with five species was adopted and tested in ref 1, and it is not clear whether the same technique can be used for very large kinetic schemes.

Charest et al.²⁴ developed a platform based on a second-order accurate finite-volume scheme. A Newton–Krylov-based implicit solver was adopted for solving the governing equations for compressible flows on multiprocessor computer architectures. Several laminar coflow flames were successfully simulated with good parallel efficiencies.

The adoption of high-order compact finite-difference spatial discretization techniques in a fully implicit solver was explored by Dobbins and Smooke²⁵ to simulate a periodically forced coflow laminar flame. Even though the calculations were performed using only a global (one-step) kinetic mechanism, it was demonstrated that all of the unsteady phenomena can be correctly captured only if a very high order spatial discretization is adopted.

In this article, we describe and analyze on a computational basis a new platform called *laminarSMOKE* for the numerical modeling of laminar flames. In particular, the present

paper extends the previous work of Cuoci et al.²⁶ in which the same platform was validated through a comparison with experimental data. The laminarSMOKE code is specifically designed to manage very detailed kinetic mechanisms (hundreds of species), and it is based on the operator-splitting methodology. The main novelty with respect to the solvers summarized above is represented by its great generality, which is achieved by the adoption of the well-known open-source OpenFOAM code²⁷ to discretize the transport equations of mass, momentum, species, and energy. The resulting code is able to model reacting flows under steady-state and unsteady conditions in complex geometries and structured and unstructured meshes, and it can be freely downloaded at the following URL: <http://www.opensmoke.polimi.it/>.

The remainder of the paper is organized as follows. In section 2 we introduce the mathematical model, that is, the governing equations that are solved by the code. The numerical methodology, which is based on the operator-splitting technique, is described in section 3. In section 4 we present several examples for which the laminarSMOKE code was successfully applied: a flat premixed flame, a counter-flow diffusion flame, a couple of laminar coflow flames under steady state or transient conditions, and a perforated plate burner. Then in section 5 the computational performances of the proposed algorithm are analyzed and discussed to demonstrate its general applicability and potential for performing large-scale, detailed combustion computations. Conclusions and future developments are briefly presented in the last section.

2. GOVERNING EQUATIONS

The numerical model presented in this work considers a reacting gas mixture in laminar conditions.²⁴ The laminarSMOKE code solves the usual conservation equations of mass, momentum, species and energy, assuming a Newtonian fluid:

$$\frac{\partial \rho}{\partial t} + \nabla(\rho \mathbf{v}) = 0 \quad (1)$$

$$\frac{\partial}{\partial t}(\rho \mathbf{v}) + \nabla(\rho \mathbf{v} \mathbf{v} + p \mathbf{I}) = \nabla \mathbf{T} + \rho \mathbf{g} \quad (2)$$

$$\frac{\partial}{\partial t}(\rho Y_k) + \nabla(\rho Y_k \mathbf{v}) = -\nabla(\rho Y_k \mathbf{V}_k) + \dot{\Omega}_k, \quad k = 1, \dots, N_C \quad (3)$$

$$\begin{aligned} \rho C_p \frac{\partial T}{\partial t} + \rho C_p \mathbf{v} \nabla T \\ = -\nabla \mathbf{q} - \rho \nabla T \sum_{k=1}^{N_C} C_{p,k} Y_k \mathbf{V}_k - \sum_{k=1}^{N_C} h_k \dot{\Omega}_k \end{aligned} \quad (4)$$

where t is the time, ρ is the mixture density, p is the pressure, \mathbf{v} is the mixture velocity, \mathbf{T} is the fluid stress tensor, \mathbf{g} is the acceleration vector due to gravity, Y_k is the mass fraction of species k , \mathbf{V}_k is the diffusion velocity of species k , $\dot{\Omega}_k$ is the formation rate of species k , T is the temperature, C_p and $C_{p,k}$ are the specific heat at constant pressure of the mixture and of species k , respectively, \mathbf{q} is the heat flux vector, h_k is the individual-species enthalpy (i.e., the sum of the sensible and formation enthalpies), and N_C is the total number of species in the kinetic scheme.

The ideal gas equation of state is used to calculate the density of the mixture. The heat flux vector accounts for conduction and radiation:

$$\mathbf{q} = -\lambda \nabla T + \mathbf{q}_{\text{rad}} \quad (5)$$

where λ is the mixture thermal conductivity and \mathbf{q}_{rad} is the radiative heat flux. The diffusion velocities are calculated by accounting for the Fick's and thermal diffusion (Soret effect):²⁸

$$\mathbf{V}_k = -\frac{D_k}{Y_k} \nabla Y_k - \frac{D_k \Theta_k}{X_k} \frac{1}{T} \nabla T \quad (6)$$

where X_k is the mole fraction and Θ_k the thermal diffusion ratio of species k and D_k is the individual-species mixture-averaged diffusion coefficient, which is related to the binary diffusion coefficients Γ_{jk} through the expression²⁹

$$D_k = \frac{1 - Y_k}{\sum_{j \neq k}^{N_C} \frac{X_k}{\Gamma_{jk}}} \quad (7)$$

The contribution due to the pressure-gradient diffusion was neglected for all of the simulations analyzed in this work. Indeed, the pressure-gradient contribution plays a very marginal role in the numerical modeling of conventional laminar flames and is usually ignored by the literature on this topic.^{14,15,22,30}

The approach proposed by Coffee and Heimerl³¹ was here adopted to enforce the mass conservation. This approach is based on a so-called *correction diffusion velocity* \mathbf{V}_k^C , which replaces \mathbf{V}_k in eqs 3 and 4 and is defined as

$$\mathbf{V}_k^C = \mathbf{V}_k + \mathbf{V}_C \quad (8)$$

where \mathbf{V}_C is a constant correction factor that is species-independent but varies in space and time. This correction factor is introduced to satisfy the mass conservation and is evaluated as

$$\mathbf{V}_C = -\sum_{k=1}^{N_C} Y_k \mathbf{V}_k \quad (9)$$

The use of Fick's law (together with the *light species approximation* for the evaluation of the thermal diffusion ratios) could lead to some inaccuracies. In such cases, a full multicomponent approach should be adopted in order to improve the accuracy and enforce the conservation of mass without additional corrections.³² The application of full multicomponent transport models is computationally very expensive, and the computational cost increases at least with the square of the number of transported species. Because of this, they have hardly been applied for the simulation of multidimensional flames.³³ To our knowledge, the most accurate simulation adopting full multicomponent transport was performed by Dworkin et al.,³⁴ who modeled an axisymmetric sooting ethylene flame using a detailed kinetic scheme with 66 species.

Most of the works on numerical simulations of laminar reacting flows have adopted mixture averaging rules, especially those based on detailed kinetic schemes, in order to save computational time. Therefore, since our simulations involve very large kinetic schemes (~200 species), we considered the mixture averaging formulation (eq 6) to be sufficiently reliable and accurate for the purposes of the present work, as is evident from the satisfactory agreement with the experimental data reported in section 4.

The radiative heat transfer was modeled by assuming the optically thin radiation hypothesis. In particular, we assumed that H₂O, CO, CO₂, and CH₄ are the only significant radiating species. Under the optically thin limit assumption (in which self-absorption of radiation is neglected), the radiative heat contribution in the energy equation can be written as

$$\nabla \mathbf{q}_{\text{rad}} = -4\sigma a_p (T^4 - T_{\text{env}}^4) \quad (10)$$

where T_{env} is the environment temperature and σ is the Stefan-Boltzmann constant. The following expression was adopted to evaluate the Planck mean absorption coefficient a_p :

$$a_p = p_{\text{H}_2\text{O}} a_{p,\text{H}_2\text{O}} + p_{\text{CO}_2} a_{p,\text{CO}_2} + p_{\text{CO}} a_{p,\text{CO}} + p_{\text{CH}_4} a_{p,\text{CH}_4} \quad (11)$$

where p_k is the partial pressure of species k . The extinction coefficient $a_{p,k}$ of species k is estimated from calculations based on the RADCAL software.³⁵

3. COMPUTATIONAL FRAMEWORK

The gas-phase transport equations reported in the previous section are solved on the top of the OpenFOAM platform.²⁷ In

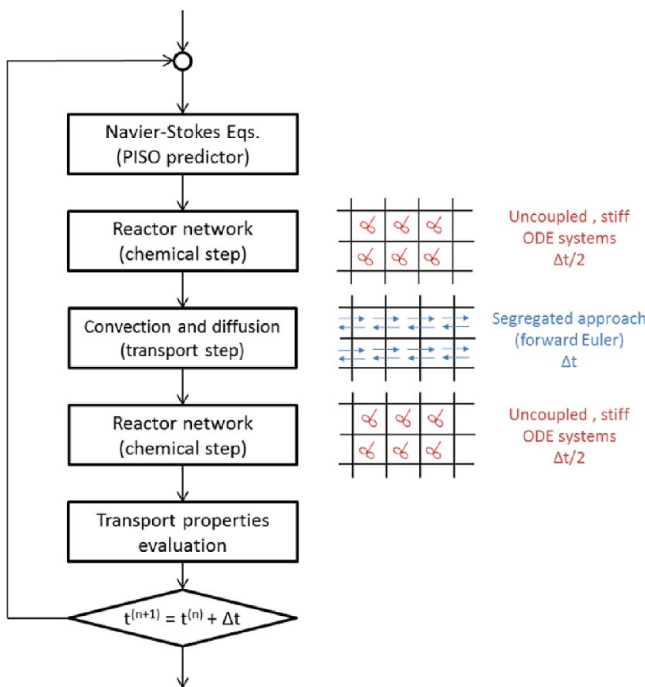


Figure 1. Numerical algorithm adopted in the laminarSMOKE code.

In particular, the laminarSMOKE code was derived from the pisoFoam solver for unsteady, compressible, nonreacting flows, which is available in the standard OpenFOAM solver collection. In order to make possible the simulation of reacting flows with detailed kinetic mechanisms, the pisoFoam solver was properly modified by introducing a so-called operator-splitting approach to properly separate the transport and reaction terms in the equations of energy and species.

3.1. Splitting Algorithm. The conventional CFD methods based on segregated algorithms are usually not suitable for solving reacting flows with detailed chemistry because of the high stiffness and the significant nonlinearities characterizing the transport equations of species and energy. In contrast,

coupled methods present several attractive numerical features for the solution of stiff, large systems of nonlinear equations. Among the others, two main approaches should be noted: (a) fully coupled methods, pioneered by Smooke et al.³⁰ in combustion and then extended by several authors^{3,5,7,9,25}, and (b) operator-splitting methods.^{22,36–39} Fully coupled algorithms treat all of the physical processes and their interactions simultaneously without introducing any decoupling between the governing equations. Thus, fully coupled methods seem to be the natural way to treat problems with multiple stiff processes, such as reactive flows in combustion. There should not be any concern, in principle, about synchronizing the interactions between the different processes, which are taken into account together. However, especially when detailed kinetics and complex, multidimensional geometries are considered, the number of coupled equations to be solved can be very large, and the requests in terms of computational resources can rapidly become prohibitive. Indeed, implicit matrix equations result from the application of fully coupled methods. Even though such matrices are usually very sparse and block-structured, a large amount of computational work goes into advancing the solution. This computational load becomes even worse when higher-order approximations to the spatial derivatives are used.³⁷ The idea on which operator-splitting methods (or fractional step methods) are based is very simple and consists of splitting the governing equations into several subequations. Each of these subequations retains only a single operator, capturing only a portion of the physics present. In particular, for combustion problems it is very convenient to separate the convective and diffusive transport terms (nonstiff processes) from the terms associated with the chemical reactions (stiff processes).^{40,41} The advantage is that in operator-splitting methods it is possible to choose the best numerical method for each type of term or process and therefore to avoid (or reduce) some expensive matrix operations typical of fully coupled algorithms. However, the formulation of a robust operator-splitting algorithm is usually more complex than the implementation of fully coupled algorithms. In particular, the best solution to split the processes is not necessarily the same for different problems or even from one situation to another.

The operator-splitting approach implemented in the laminarSMOKE code is briefly summarized in the following. The method of lines (MOL) is taken into account, which means that after the spatial discretization, the transport equations of species and energy are rewritten in the general form⁴²

$$\frac{d\psi}{dt} = \mathbf{C}(\psi, t) + \mathbf{D}(\psi, t) + \mathbf{R}(\psi) \quad (12)$$

where ψ is the vector of mass fractions and temperature (i.e., the primary variables), $\mathbf{C}(\psi, t)$ and $\mathbf{D}(\psi, t)$ are the vectors of rates of change of ψ due to the transport (i.e., convection and diffusion, respectively), and $\mathbf{R}(\psi)$ is the vector of rates of change of ψ due to chemical reactions. The numerical solution of eq 12 is obtained by discretizing the time in increments Δt and advancing the solution on each of these time steps. Each of the terms on the right-hand side of eq 12 contributes some amount to the overall change in ψ during the numerical time step. Thus:

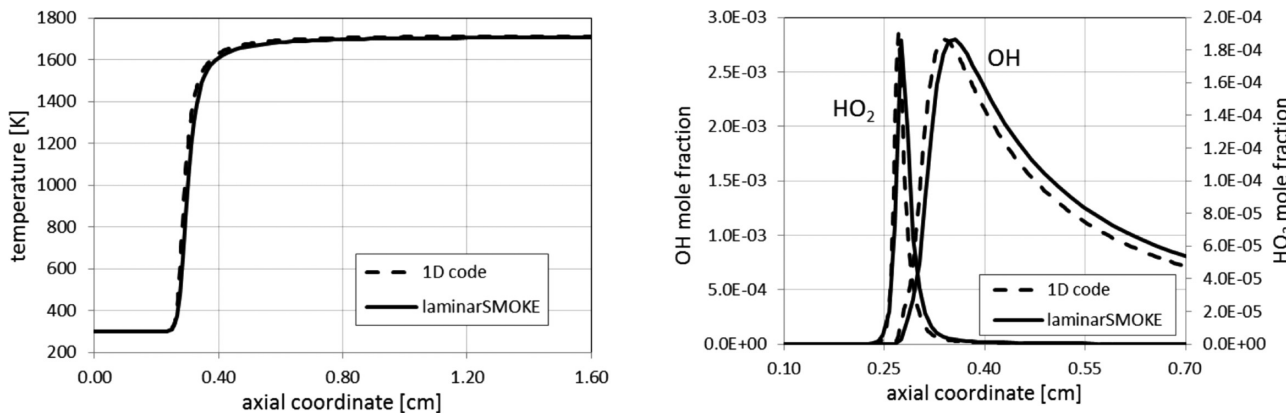


Figure 2. Laminar premixed flame (1D): comparison between numerical solutions (dashed lines, OpenSMOKE code;^{48,49} solid lines, laminarSMOKE code).

$$\begin{cases} \frac{d\psi}{dt} \Big|_i = C(\psi, t) \\ \frac{d\psi}{dt} \Big|_{ii} = D(\psi, t) \\ \frac{d\psi}{dt} \Big|_{iii} = R(\psi) \end{cases} \quad (13)$$

The solution is found by summing all of the partial contributions reported above. Several variations in the sequence corresponding to eq 13 are possible, with different accuracies and stability properties, as deeply studied in refs 38, 40, and 43. In particular, it was demonstrated that especially when complex kinetic mechanisms are involved, the stiff (chemistry) operator always has to be the last in the splitting process in order to ensure satisfactory stability and accuracy. According to these observations, in the present work the Strang splitting scheme⁴⁴ is adopted, in which the convection and diffusion terms are grouped together and separated from the stiff chemical reaction term. The numerical integration is then performed in three substeps:

Substep 1. First of all, the reaction term is integrated over the time step $\Delta t/2$ by solving the following stiff ordinary differential equation (ODE) system:

$$\frac{d\psi^a}{dt} = R(\psi^a) \quad (14)$$

The initial condition $\psi^a(0)$ corresponds to the final state from the previous time step, and the solution of eq 14 is denoted as $\psi^a(\Delta t/2)$.

Substep 2. The convection and diffusion terms are integrated along the whole time step Δt by solving the following ODE system:

$$\frac{d\psi^b}{dt} = C(\psi^b, t) + D(\psi^b, t) \quad (15)$$

The initial condition $\psi^b(0)$ is equal to the final state of the system from substep 1, $\psi^a(\Delta t/2)$, and the solution of eq 15 is denoted as $\psi^b(\Delta t)$.

Substep 3. This last step is identical to the first substep, except that the initial condition corresponds to the final state of the system from substep 2, $\psi^b(\Delta t)$. The solution is then used as the initial condition for the next time step.

Substeps 1 and 3 (the reaction steps) have no spatial dependence and do not require boundary conditions. On the contrary, the transport operators $C(\psi, t)$ and $D(\psi, t)$ do have spatial dependence and thus require the application of appropriate boundary conditions. As a consequence, there are N (where N is the total number of computational cells) stiff ODE systems corresponding to substeps 1 and 3, which are completely independent (i.e., decoupled) and can be solved in sequence. The number of unknowns for each ODE system is relatively small and equal to $N_C + 1$. The features of the ODE system corresponding to substep 2 (transport) are quite different. This ODE system is quite large, since it involves $N(N_C + 1)$ coupled equations. However, these equations are not stiff, which means that a segregated approach can be used to solve them. In other words, the following approximation can be adopted: instead of solving the whole ODE system, $N_C + 1$ independent ODE systems are solved in sequence, each of them having dimension equal to N . The spatial discretization of convection and diffusion terms uses the numerical tools available in the OpenFOAM platform. The nonstiff ODE systems (eq 15) are solved using the backward (or implicit) Euler method. Iterative techniques are employed to solve the linear systems involved in the ODE solution, which consist of the sequential reduction of the equation residual over a succession of solutions.⁴⁵ While the Poisson equation for the pressure is solved using the preconditioned conjugate gradient (PCG) method (because of the symmetry of the corresponding linear system), all of the remaining linear systems are solved using the preconditioned biconjugate gradient (PBiCG) method. The diagonal incomplete Cholesky (DIC) technique is adopted to precondition the PCG solver, while the diagonal incomplete LU (DILU) technique is used to precondition the PBiCG solver. The iterative sequence stops under one of the following conditions: (i) the ratio of the current and initial residuals is reduced below the prescribed relative tolerance, (ii) the residual falls below the prescribed absolute tolerance, or (iii) the maximum number of iterations is reached. For the flames investigated in the present work, when the time step is properly chosen (corresponding to a maximum Courant's number of 0.1), the number of iterations needed by the transport equations of momentum, energy, and species is usually quite small (3–4 iterations at maximum). A larger number of iterations is required by the pressure equation (usually 20–30). Thus, the maximum number of iterations is fixed by the user by taking into account these observations. In

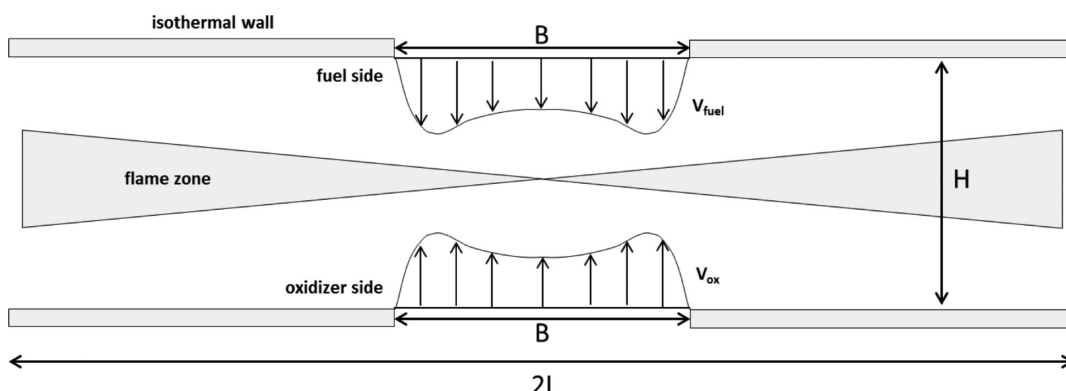
Table 1. Laminar Premixed Flame (1D): Grid Convergence Analysis (Steady-State Solution)

	maximum values ^a				mean values ^b		Rn
	n = 1	n = 2	n = 4	∞	p	GCI (%)	
T (K)	1707.4	1712	1714.1	1715	1.54	0.05	70%
H ₂	7.99 × 10 ⁻³	8.22 × 10 ⁻³	8.29 × 10 ⁻³	8.33 × 10 ⁻³	1.56	0.48	73%
O ₂	3.21 × 10 ⁻⁵	3.29 × 10 ⁻⁵	3.32 × 10 ⁻⁵	3.33 × 10 ⁻⁵	1.55	0.44	68%
H ₂ O	1.48 × 10 ⁻¹	1.49 × 10 ⁻¹	1.50 × 10 ⁻¹	1.50 × 10 ⁻¹	1.64	0.15	71%
OH	2.76 × 10 ⁻³	2.80 × 10 ⁻³	2.81 × 10 ⁻³	2.82 × 10 ⁻³	1.35	0.35	65%
H ₂ O ₂	1.12 × 10 ⁻⁴	1.23 × 10 ⁻⁴	1.26 × 10 ⁻⁴	1.28 × 10 ⁻⁴	1.50	1.59	60%
HO ₂	1.15 × 10 ⁻⁵	1.25 × 10 ⁻⁵	1.28 × 10 ⁻⁵	1.30 × 10 ⁻⁵	1.57	1.34	63%
H	1.77 × 10 ⁻⁴	1.90 × 10 ⁻⁴	1.95 × 10 ⁻⁴	1.97 × 10 ⁻⁴	1.49	1.36	60%
O	1.47 × 10 ⁻³	1.56 × 10 ⁻³	1.60 × 10 ⁻³	1.62 × 10 ⁻³	1.47	1.19	61%

^aFor H₂ and O₂, the values at the outlet boundary are reported instead of the maximum values. ^bGlobal values of p and GCI were calculated by means of arithmetic and volumetric averaging, respectively.

Table 2. Laminar Premixed Flame (1D): Convergence Analysis with Respect to the Time Step Using the Temperature and Mole Fractions Evaluated at the Point with Axial Coordinate Equal to 4.50 mm at Time t = 1 s

	n = 1	n = 2	n = 4	∞	p
T (K)	1658.9	1661.1	1661.9	1662.5	1.32
H ₂	1.11 × 10 ⁻²	1.10 × 10 ⁻²	1.09 × 10 ⁻²	1.09 × 10 ⁻²	1.36
O ₂	1.90 × 10 ⁻³	1.83 × 10 ⁻³	1.80 × 10 ⁻³	1.78 × 10 ⁻³	1.37
H ₂ O	1.94 × 10 ⁻¹	1.95 × 10 ⁻¹	1.95 × 10 ⁻¹	1.95 × 10 ⁻¹	1.29
OH	1.71 × 10 ⁻³	1.67 × 10 ⁻³	1.66 × 10 ⁻³	1.65 × 10 ⁻³	1.32
H ₂ O ₂	5.54 × 10 ⁻⁷	5.22 × 10 ⁻⁷	5.08 × 10 ⁻⁷	4.97 × 10 ⁻⁷	1.22
HO ₂	6.10 × 10 ⁻⁷	5.81 × 10 ⁻⁷	5.69 × 10 ⁻⁷	5.59 × 10 ⁻⁷	1.15
H	1.78 × 10 ⁻³	1.72 × 10 ⁻³	1.69 × 10 ⁻³	1.67 × 10 ⁻³	1.25
O	2.03 × 10 ⁻⁴	1.92 × 10 ⁻⁴	1.88 × 10 ⁻⁴	1.84 × 10 ⁻⁴	1.22

**Figure 3.** Geometry of the 2D planar opposed-jet diffusion burner (adapted from ref 53).

the very uncommon case that the maximum number of iterations is reached, a warning message is reported by the laminarSMOKE code in order to give the user the opportunity to investigate the reasons for the failure and to review the numerical options. In most cases it is sufficient to reduce the time step.

Only the species and energy equations are solved through the Strang splitting algorithm. Since the continuity and momentum equations are solved in a segregated approach, in order to ensure the conservation of mass at each time step, the pressure implicit with splitting of operators (PISO) algorithm is applied. This algorithm, first introduced by Issa,⁴⁶ was found to be sufficiently accurate and fast for all of the cases investigated in the present work. In order to avoid stability issues, the time step is automatically adjusted during the calculations to have a sufficiently small maximum Courant number. Figure 1 depicts the whole numerical procedure here adopted.

3.2. Detailed Kinetic Mechanisms. Several detailed kinetic mechanisms developed by the CRECK Modeling Group at the Politecnico di Milano and extensively described and validated in refs 47 and 48 were used to perform the calculations reported in this work. In particular, the Polimi_H2CO1212 mechanism (14 species and 37 reactions) was used for the simulation of laminar premixed flames described in section 4.1, while the POLIMI_C1C31212 scheme (82 species and 1495 reactions) and the more general POLIMI_HT1212 scheme (198 species and 6307 reactions, considering also the formation of soot precursors) were used for the diffusion flames. All of the kinetic mechanisms are available in CHEMKIN format and can be freely downloaded at the following URL: <http://creckmodeling.chem.polimi.it/>.

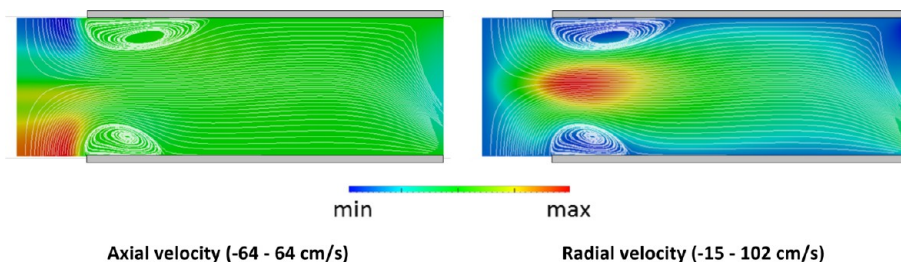


Figure 4. Counter-flow diffusion flame: calculated maps of axial and radial velocities together with the stream lines under steady-state conditions. The simulation was performed on a computational mesh with 78 720 cells using the POLIMI_C1C31212 kinetic mechanism.⁴⁸ The numbers reported in parentheses are the minimum and maximum values.

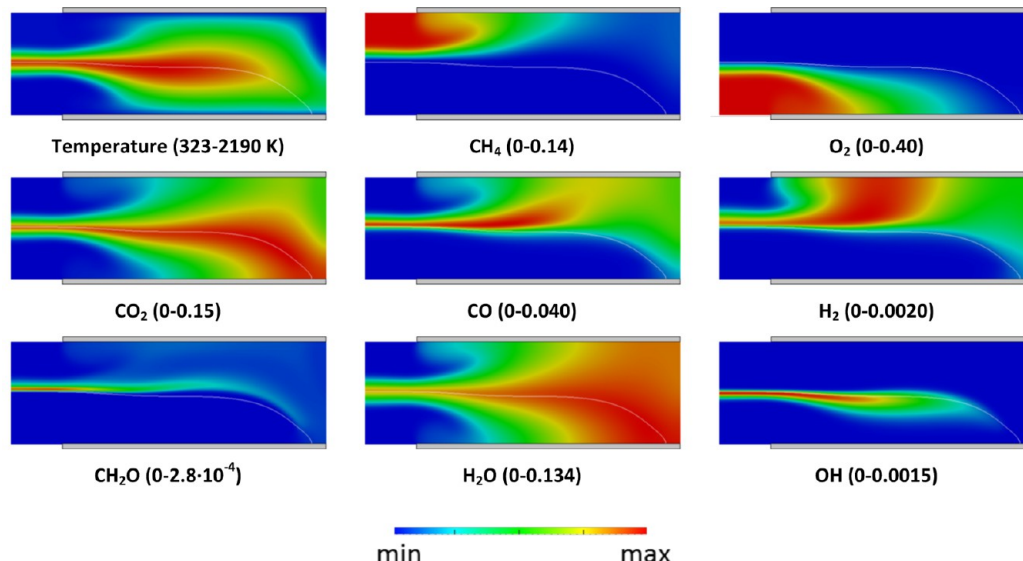


Figure 5. Counter-flow diffusion flame: calculated maps of temperature and mass fractions of main species under steady-state conditions. The simulation parameters are the same as in Figure 4. The numbers reported in parentheses are the minimum and maximum values.

4. NUMERICAL RESULTS

In this section we present five different simulations to validate the numerical procedure described in the previous section. Since the discretization of the transport equations is managed by the OpenFOAM platform, the laminarSMOKE solver is

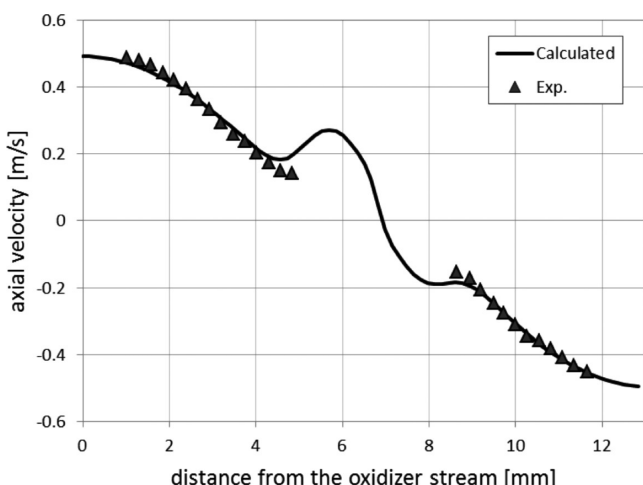


Figure 6. Counter-flow diffusion flame: comparison between the experimental⁵² and calculated axial velocity profiles along the axis of symmetry. The simulation parameters are the same as in Figure 4.

able to simulate reacting flows under both steady-state and unsteady conditions on arbitrarily complex geometries (1D, 2D, and 3D). However, in this work we focused our attention only on simple geometries, without exploring and exploiting all of the available features and capabilities. In the first example, we modeled a premixed flame fed with CH_4 and air, using the results to illustrate the convergence properties of the proposed algorithm. The second example focused on the numerical modeling of a counterflow diffusion flame in an axisymmetric domain. Both steady-state and unsteady conditions were simulated, a convergence analysis was performed, and a comparison with experimental measurements was made. In the third example, a series of laminar coflow flames fed with a partially premixed mixture of CH_4 and air with different equivalence ratios (from $\phi = \infty$ to $\phi = 2.5$) were modeled using a very detailed kinetic mechanism (~200 species), accounting also for the formation of soot precursors. The numerical results were compared with the measurements and showed very satisfactory agreement, providing a complete validation of the solver. In the fourth example, a diffusion flame fed with CH_4 and N_2 was modeled under both steady-state conditions and unsteady conditions (i.e., by imposing a sinusoidal perturbation on the fuel inflow velocity). Finally, a premixed laminar flame was also simulated using the laminarSMOKE code. In particular, the attention was focused on a perforated plate burner consisting of drilled holes arranged in a honeycomb structure.

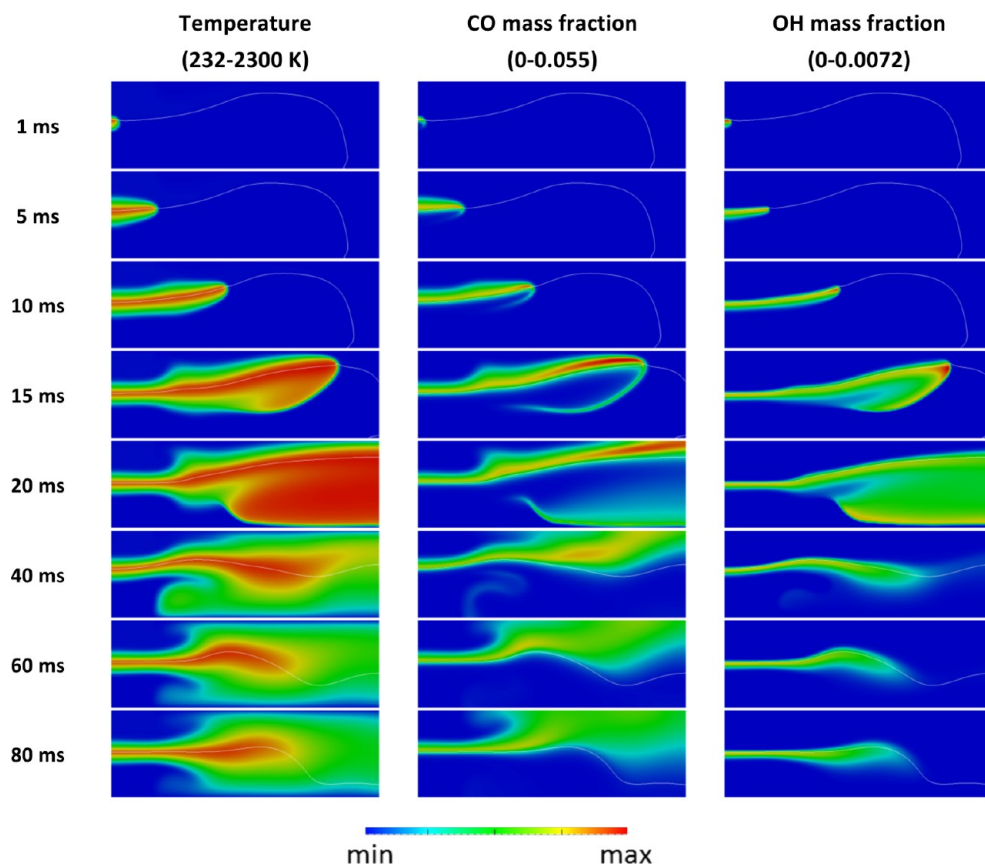


Figure 7. Counter-flow diffusion flame: calculated maps of temperature and mass fractions of CO and OH at different times, counted from the time of ignition. The continuous lines represent the flame front (i.e., where the mixture fraction has the stoichiometric value of 0.416). The simulation parameters are the same as in Figure 4.

An Infiniband platform was used to run all of the simulations. In its current configuration, it is made up of 16 nodes, each having 36 GB of RAM and 12 Intel Xeon X5675 processors (12Mb cache, 3.06 GHz, 6.40 GT/s Intel QPI).

The steady-state simulations described in the following were actually calculated by simulating the transient behavior of the system for a sufficiently long period of time until it reached a steady state. The steady-state conditions were detected by looking at proper norms of the residuals of equations and by monitoring the solution at fixed points in the computational domain versus the number of time steps.

The simulations reported in the following were performed using a centered spatial scheme and a maximum Courant number of 0.1.

4.1. Premixed Flames (1D). As a first example, we performed the numerical simulation of several flat, 1D laminar premixed flames. This choice was made for the following two main reasons: (i) since the problem is 1D, we have the possibility to compare the numerical solution obtained using *laminarSMOKE* with the fully coupled solution obtained with the *OpenSMOKE* code;^{48,49} (ii) since a complete analysis requires a large number of simulations (as better explained in the following), a simple 1D problem allowed us to save a lot of computational time.

Even though the tests were conducted on several flames with different inlet compositions and operating conditions, here we report only the results corresponding to a flame fed with a mixture of H₂ (19.09%), O₂ (9.10%), and N₂ (71.81%) at a temperature of 298 K, atmospheric pressure, and a velocity of

57.3 cm/s. On the basis of the work of Day and Bell,²² a non-equispaced 1D computational mesh with 600 cells (corresponding to a minimum spacing of 0.01 mm) was adopted to perform the simulations. The chemistry was described with the Polimi_H2CO1212 kinetic scheme,⁵⁰ and a centered second-order discretization scheme was adopted for the spatial discretization of the transport equations of species and temperature. The *laminarSMOKE* solution was compared with a fully coupled solution obtained using the *OpenSMOKE* code. The comparison between the two solutions is reported in Figure 2 in terms of profiles of temperature and mass fractions of OH and HO₂. As is evident, the agreement is quite satisfactory. In particular, the maximum relative errors between the two solutions are ~0.45% for the temperature and ~0.23% and ~0.70% for the OH and HO₂ mole fractions, respectively. The splitting error in the *laminarSMOKE* solver can be considered the main source of error responsible for the observed differences. All of the remaining species in the kinetic mechanism showed similar behavior, which is not here reported because of the lack of space.

In order to complete the analysis and study the sensitivity of the results to the mesh spacing, we performed additional tests, as suggested by Roache.⁵¹ In particular, the order of accuracy of the numerical solution (p) and the uncertainty due to discretization (i.e., the error band in which the grid-independent solution is expected to be contained) were investigated through the generalized Richardson extrapolation for h-refinement studies and the grid convergence index (GCI). Three levels of refinement ($n = 1, 2$, and 4, corresponding to

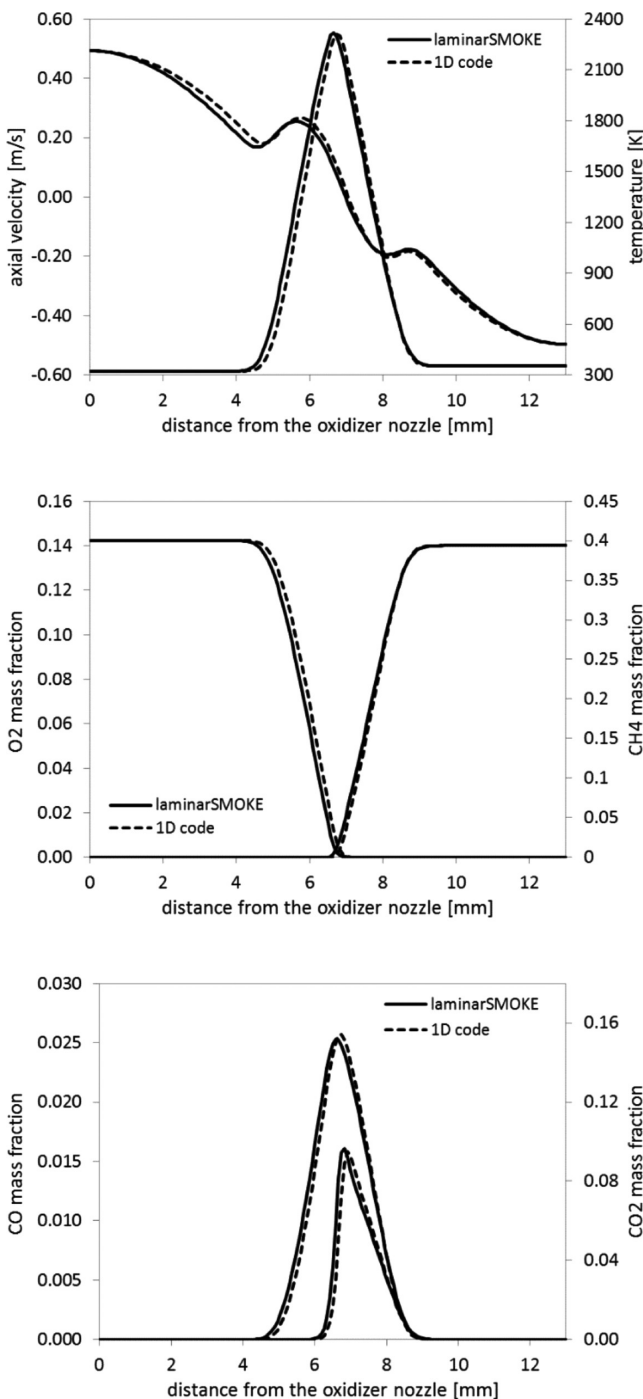


Figure 8. Counter-flow diffusion flame: comparison between the laminarSMOKE code and the OpenSMOKE 1D code^{48,49} in terms of profiles of temperature, axial velocity, and mass fraction of main species along the axis of symmetry. The simulation parameters are the same as in Figure 4.

Table 3. Counter-Flow Diffusion Flame: Computational Meshes Used for the Numerical Simulations

	axial cells	radial cells	cell dimensions	number of cells
mesh A	40	123	325 μm × 325 μm	4920
mesh B	80	246	162.5 μm × 162.5 μm	19680
mesh C	160	492	81.25 μm × 81.25 μm	78720

300, 600, and 1200 grid cells) were considered for these studies. Only the grid nodes where monotone convergence was observed (also defined as Richardson nodes) were considered for estimating p and the GCI. A sufficiently high percentage (60%) of Richardson nodes (R_n) was found. The main results of this analysis are summarized in Table 1. In particular, we report p and the GCI for all species and the temperature. Even though a second-order discretization scheme was adopted, we found that the real order of convergence accuracy (p) was between 1.35 and 1.65. Considering the stretch of the computational mesh and the strong nonlinearities of the reaction terms in the transport equations of species and temperature, these results are not bad. The whole procedure can be considered sufficiently reliable and correctly applied, since the resulting GCI was sufficiently small. As an example, the average uncertainty of temperature was equal to 0.050%, corresponding to ± 0.80 K with respect to the maximum value.

In order to investigate the accuracy of temporal discretization, we looked at the solution at the point $x = 4.50$ mm on the coarsest grid (300 points) at time $t = 1$ s. We performed calculations up to that time using three different fixed time steps ($n = 1, 2$, and 4, corresponding to 10^{-5} , 0.5×10^{-5} , and 0.25×10^{-5} s). The convergence of temperature and mole fractions of selected species at $x = 4.50$ mm and $t = 1$ s as the time step is reduced is summarized in Table 2. Even though for all of the variables under investigation a monotonic convergence was observed, p was quite small (with values around 1.20–1.40). The expected order of convergence for the Strang splitting algorithm is much larger and equal to 2. This difference could be attributed not only to the strong nonlinearities in the source terms of the governing equations but also to the segregated approach based on the PISO algorithm that was applied to solve momentum and continuity equations, which adds a further degree of decoupling (i.e., a sort of additional splitting). Additional tests and investigations should be performed in order to better understand this point and improve the order of convergence with respect to the time step.

4.2. Counter-Flow Diffusion Flame (2D). As a second example, a laminar counter-flow diffusion flame fed with methane diluted in nitrogen and O₂-enriched air was simulated. This flame was studied previously both experimentally and numerically by Amantini et al.⁵² A schematic representation of the geometry of the burner is shown in Figure 3. The system consists of a couple of circular nozzles of internal radius (B) equal to 6.5 mm with a separation distance (H) of 13 mm. The CH₄/N₂ mixture (14%/86% by mass) flows from the top nozzle at the temperature $T_{\text{fuel}} = 353$ K and mean velocity $v_{\text{fuel}} = 46.4$ cm/s, while the O₂/N₂ mixture (40%/60% by mass) flows from the bottom nozzle at $T_{\text{ox}} = 323$ K and mean velocity $v_{\text{ox}} = 46.1$ cm/s. The nozzles are surrounded by water-cooled flanges in order to maintain a constant wall temperature (T_{wall}) of 323 K and to provide well-specified boundary conditions. The Reynolds number Re is defined as suggested in ref 53:

$$Re = \frac{\rho_{\text{ox}} v_{\text{ox}} B}{\mu_{\text{ox}}} \quad (16)$$

where ρ_{ox} and μ_{ox} are the density and the dynamic viscosity, respectively, of the oxidizer stream. The resulting Reynolds number is equal to ~ 120 , corresponding to laminar conditions. Because of the symmetry of the geometry, the system can be described using a 2D axisymmetric mesh covering a region of

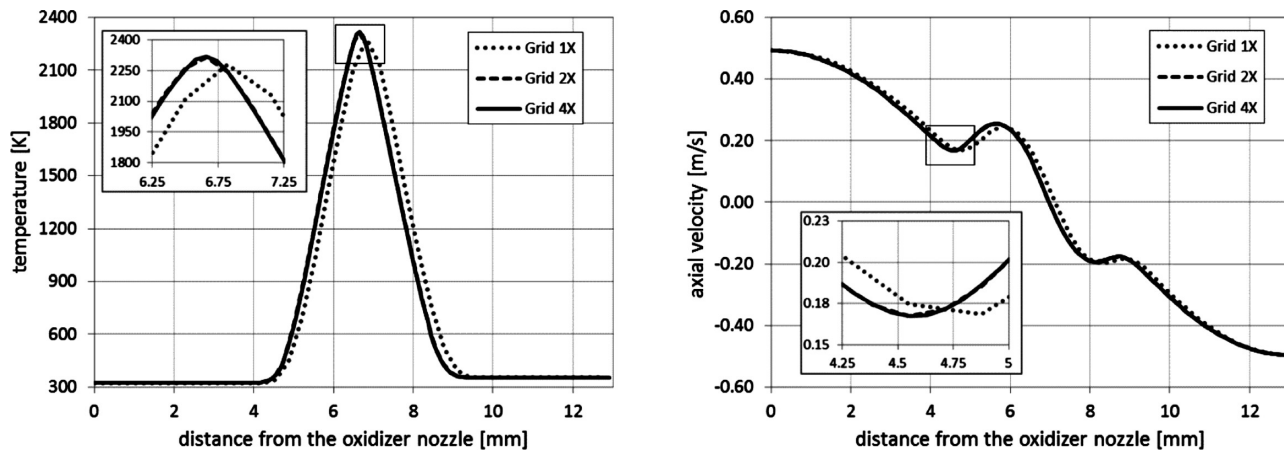


Figure 9. Counter-flow diffusion flame: effect of the grid refinement on the (left) temperature and (right) axial velocity profiles along the axis of symmetry. The simulations were performed using a three-step global mechanism.⁵⁵

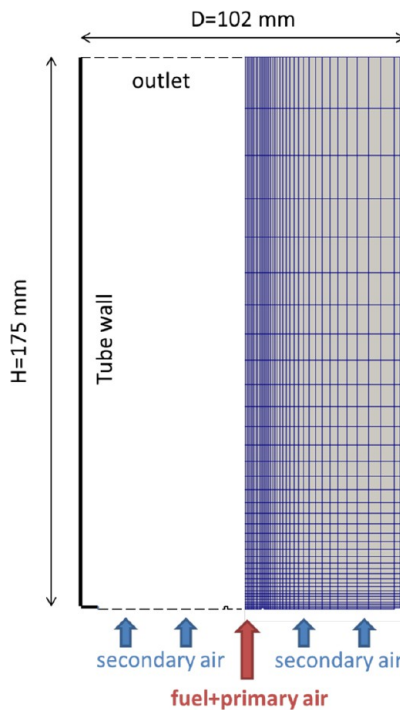


Figure 10. Partially premixed CH₄/air coflow flames: schematic of the diffusion flame setup (left side) and computational mesh (right side). The computational mesh reported here has only 1000 cells to show the regions in which the nonuniformities occur.

40 mm × 13 mm. At the walls we imposed the classical no-slip boundary conditions and fixed the temperature at the value of

Table 5. Partially Premixed CH₄/Air Coflow Flames: Flame Heights and Peak Temperatures^a

ϕ	H_{exp} (mm)	H_{calc} (mm)	T_{exp} (K)	T_{calc} (K)
∞	57	59	1960	1950
12.3	52	53	2000	1983
6.2	49	51	2020	2000
4.1	45	45	2040	2035
3.1	42	41.5	2060	2002
2.5	38	39	2090	2080

^a ϕ is the calculated primary equivalence ratio. H_{exp} and H_{calc} are the measured⁵⁶ and calculated axial positions of the maximum centerline gas temperature, respectively. T_{exp} and T_{calc} are the measured⁵⁶ and calculated maximum centerline gas temperatures, respectively.

the water-cooled flanges. At the outlet, all of the normal derivatives were set equal to zero. At the fuel and oxidizer inlets, flat profiles for the mass fractions of CH₄, O₂ and N₂ were imposed. According to experimental evidence, the radial component of the inlet velocities can be assumed to be negligible. On the contrary, the axial component varies with the radial coordinate (r) according to the following analytic form obtained by Amantini et al.:⁵²

$$\frac{v(r)}{v_{\text{mean}}} = 1.068 + 1.458 \left(\frac{r}{B} \right)^2 - 7.809 \left(\frac{r}{B} \right)^4 + 36.99 \left(\frac{r}{B} \right)^6 - 74.35 \left(\frac{r}{B} \right)^8 + 55.88 \left(\frac{r}{B} \right)^{10} - 13.20 \left(\frac{r}{B} \right)^{12} \quad (17)$$

Table 4. Partially Premixed CH₄/Air Coflow Flames: Composition and Velocity of the Inlet Streams^a

ϕ	Q_{CH_4} (cm ³ /min)	Q_p (cm ³ /min)	Q_s (cm ³ /min)	Q_{Ar} (cm ³ /min)	Re	V_{fuel} (cm/s)	V_{coflow} (cm/s)
∞	330	0	44000	3.3	38	5.68	10.49
12.3	330	210	44000	5.5	62	9.30	10.49
6.2	330	420	44000	7.6	86	12.91	10.49
4.1	330	630	44000	9.7	110	16.53	10.49
3.1	330	830	44000	11.8	133	20.15	10.49
2.5	330	1,050	44,000	14	158	23.77	10.49

^a ϕ is the calculated primary equivalence ratio. The measured⁵⁶ volumetric flow rates at STP of CH₄ (Q_{CH_4}), primary air (Q_p), secondary air (Q_s), and Ar (Q_{Ar}) are reported. Re is the Reynolds number for the fuel flow rate. V_{fuel} and V_{coflow} are the mean inlet velocities of the fuel and coflow streams.

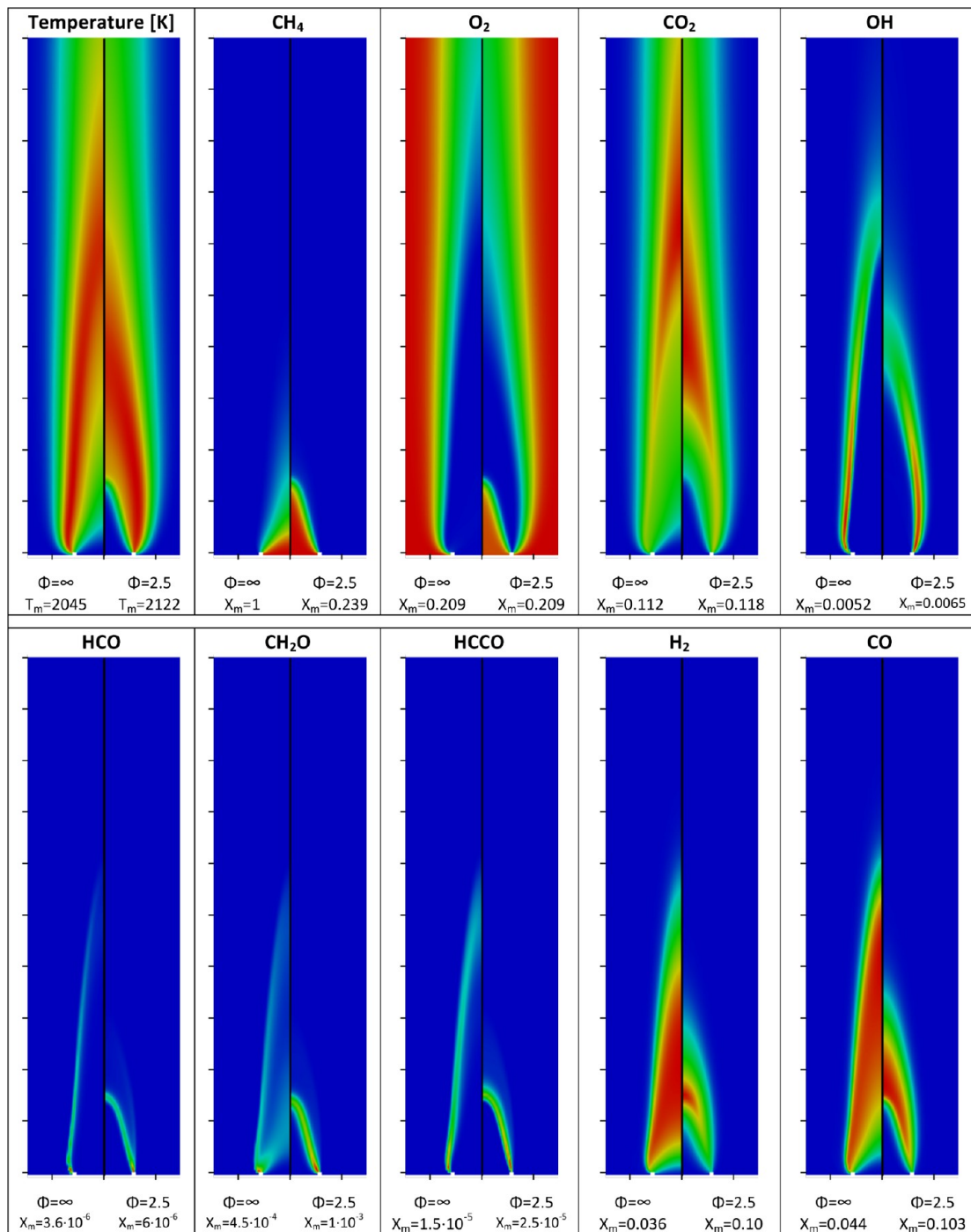


Figure 11. Partially premixed CH₄/air coflow flames: calculated maps (from 0 to 15 mm in the radial direction and from -1 to 100 mm in the axial direction) of temperature and mole fractions of selected species for flames at (left) $\phi = \infty$ and (right) $\phi = 2.5$. For each map, the maximum value (T_m or X_m) is reported (the minimum is 300 K for temperature and zero for species). The distance between the ticks is 1 cm.

In particular, these profiles result in peak velocities (on the axis of symmetry) equal to 49.55 and 49.23 cm/s for the fuel and the oxidizer nozzles, respectively.

As better explained in the following, three different structured equispaced meshes with an increasing number of cells (from ~ 5000 to $\sim 79\,000$) were tested. Moreover, the simulations were performed by employing several kinetic mechanisms. For all of the computed cases, a cold-flow solution was first obtained (representing the mixing problem between the fuel and the oxidizer streams). The ignition process was then simulated by the introduction of a spark (i.e.,

a hot spot) around the stagnation plane along the axis of symmetry. The calculations were then advanced up to the steady-state conditions. To check the convergence to the steady-state conditions, the temperature and the mass fractions of selected species (CH₄, O₂, H₂O, and OH) were monitored at three different fixed points in the computational domain. About 0.5 s of physical time (measured from the ignition) were sufficient to reach steady-state conditions. The typical adopted time step on the finest grid was equal to 10 μ s, corresponding to a Courant number of 0.1. The required CPU time per time step strongly depended on the kinetic scheme adopted (as

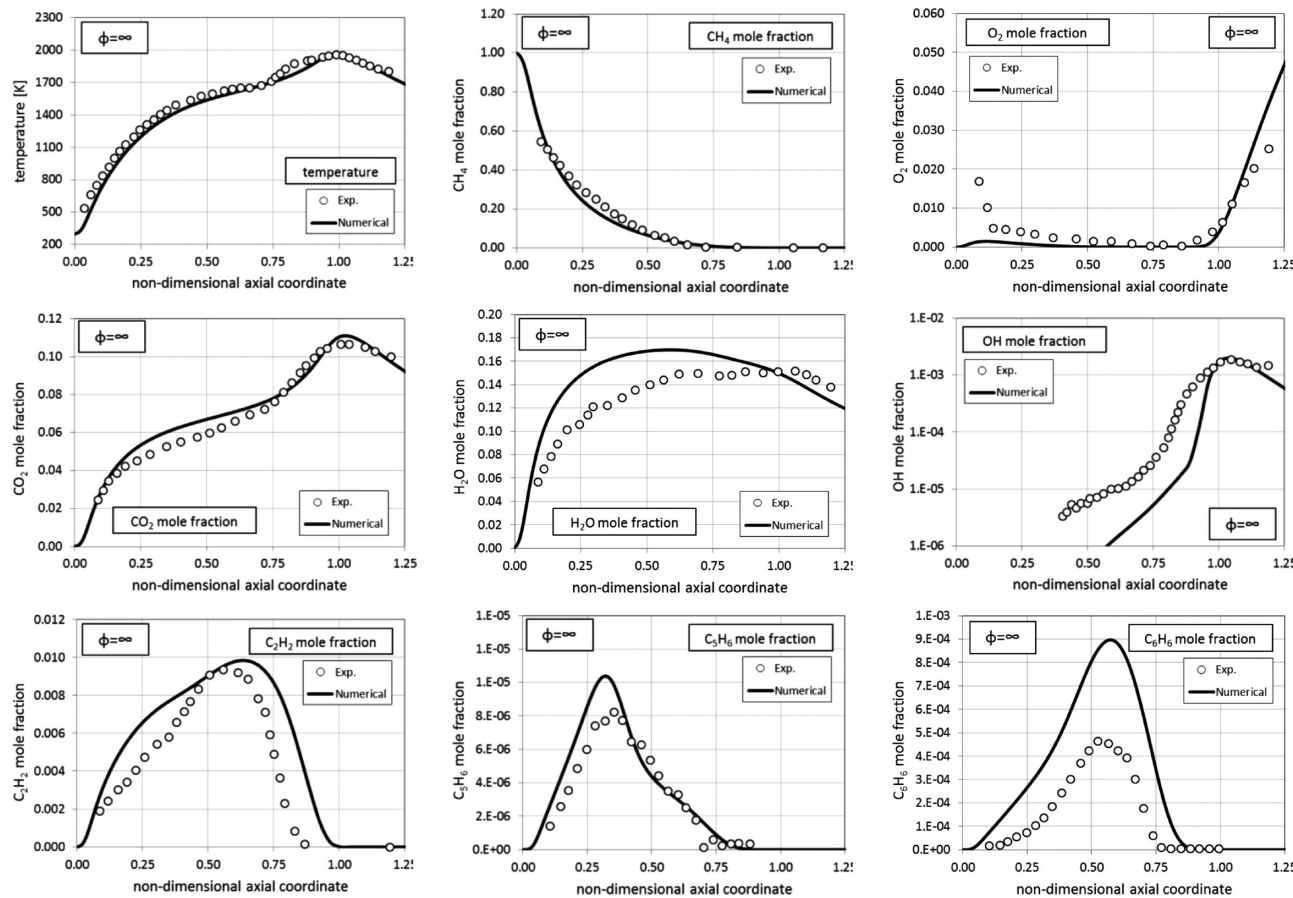


Figure 12. Partially premixed CH₄/air coflow flame at $\phi = \infty$: comparison between measurements (points)⁵⁶ and calculations (solid lines) along the centerline.

reported in Table 6) and is discussed in more detail in section 5.1.

Figure 4 presents the maps of axial and radial velocities together with the stream lines under steady-state conditions. The calculations were performed using the POLI-MI_C1C31212 detailed kinetic scheme (82 species and 1485 reactions) on a computational mesh with 78 720 cells. Two recirculation zones can be observed at the exits of the top (fuel) and bottom (oxidizer) nozzles, with characteristic lengths of ~ 11 and ~ 7 mm, respectively. The flow separation and therefore the formation of recirculation zones are a direct consequence of the sharp corners at the burner inlets. As better explained by Amantini et al.,⁵² their features are strongly affected not only by the momentum ratio between the fuel and the oxidizer streams but also by the buoyancy. The maps of temperature and mass fractions of the main species are reported in Figure 5. The continuous line represent the flame front (i.e., where the mixture fraction is equal to the stoichiometric value of 0.416). The flame is located on the fuel side, as is evident from the positions of the peak of temperature and the stagnation plane along the axis of symmetry (located ~ 6 mm from the fuel nozzle). Two regions with different features are evident: a radial development region (initially confined between the two recirculation zones) and a counter-flow region between the two nozzles. The reactants and products are transported back to the inlets of the burner from the outer periphery. The reactant species are burned, and therefore, their concentrations decrease along the radial direction. Figure 6 shows a comparison between the calculated and measured profiles⁵²

of the axial velocity along the axis. The agreement is satisfactory and demonstrates the reliability of the proposed solution. The effect of the outflow boundary condition on the solution was also analyzed by increasing the length of the computational domain from 40 to 70 mm. The corresponding results (in terms of temperature and mass fractions) show a negligible difference between the two simulations, especially along the axis of symmetry. In order to complete the analysis, the ignition process (simulated to reach the steady-state conditions) is shown in Figure 7, where maps of the temperature and the mass fractions of CO and OH at different time steps are reported. As already reported, the ignition was simulated through a temperature hot spot (at 1800 K) with a diameter equal to 0.5 mm and a duration of 1 ms located on the axis of the system. From the results it is evident that during the first 15 ms the flame front develops along the surface were the mixture fraction has the stoichiometric value. The recirculation zones then convect back the hot products, increasing the size of the flame region.

The laminarSMOKE predictions were then compared with the results obtained using OpenSMOKE, a 1D code based on a similarity solution (based on the introduction of a stream function, as suggested in ref 54), with the aim to better test the reliability of the numerical solution. Of course, the same kinetic mechanism and the same transport properties were adopted in the two calculations, and identical boundary conditions were used. Figure 8 illustrates the profiles of temperature, velocity, and mass fractions of the main species along the axis of symmetry for the laminarSMOKE and 1D codes. Even

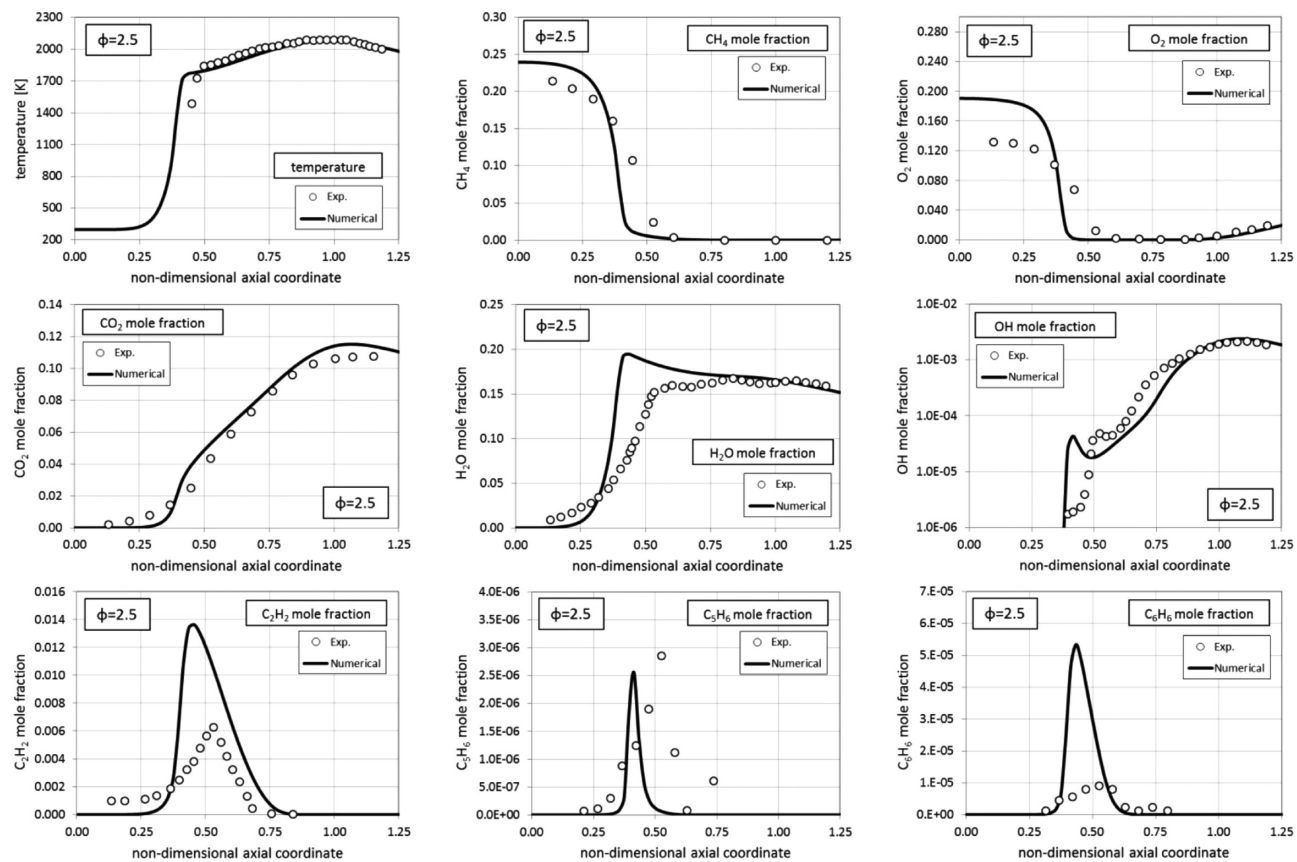


Figure 13. Partially premixed CH_4 /air coflow flame at $\phi = 2.5$: comparison between measurements (points)⁵⁶ and calculations (solid lines) along the centerline.

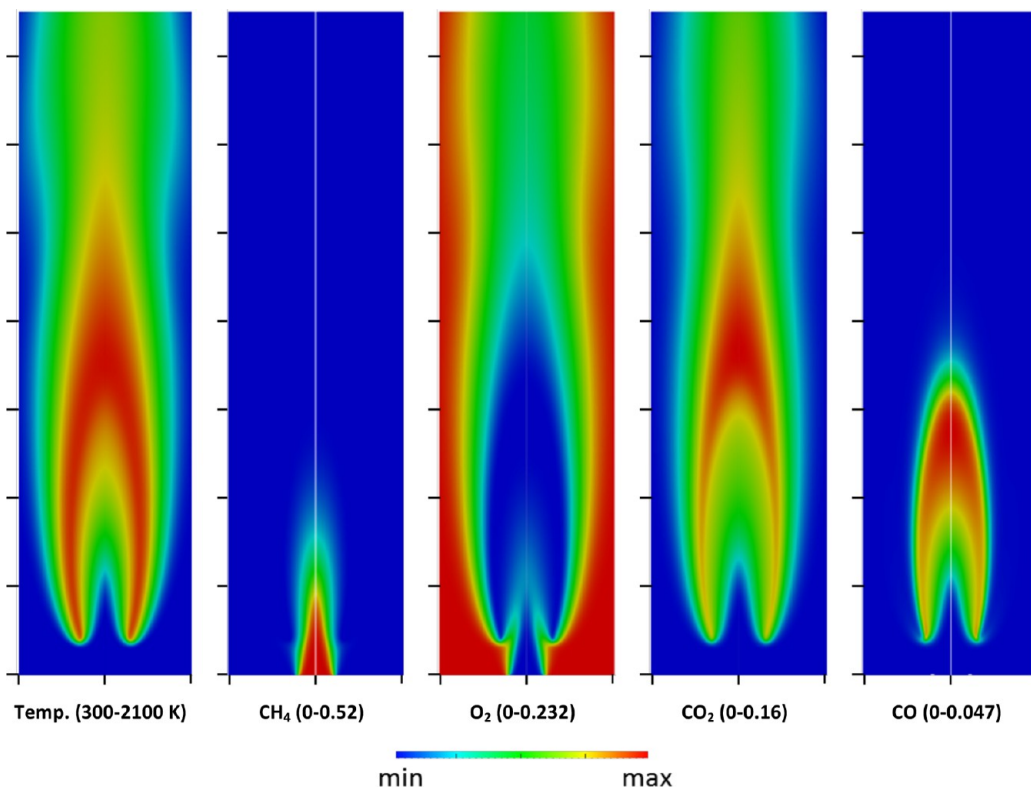


Figure 14. CH_4/N_2 coflow diffusion flame: calculated maps of temperature and mass fractions of selected species. The calculations refer to steady-state conditions. The calculated maps cover a $20 \text{ mm} \times 750 \text{ mm}$ rectangular region. The distance between the ticks on each map is equal to 1 cm.

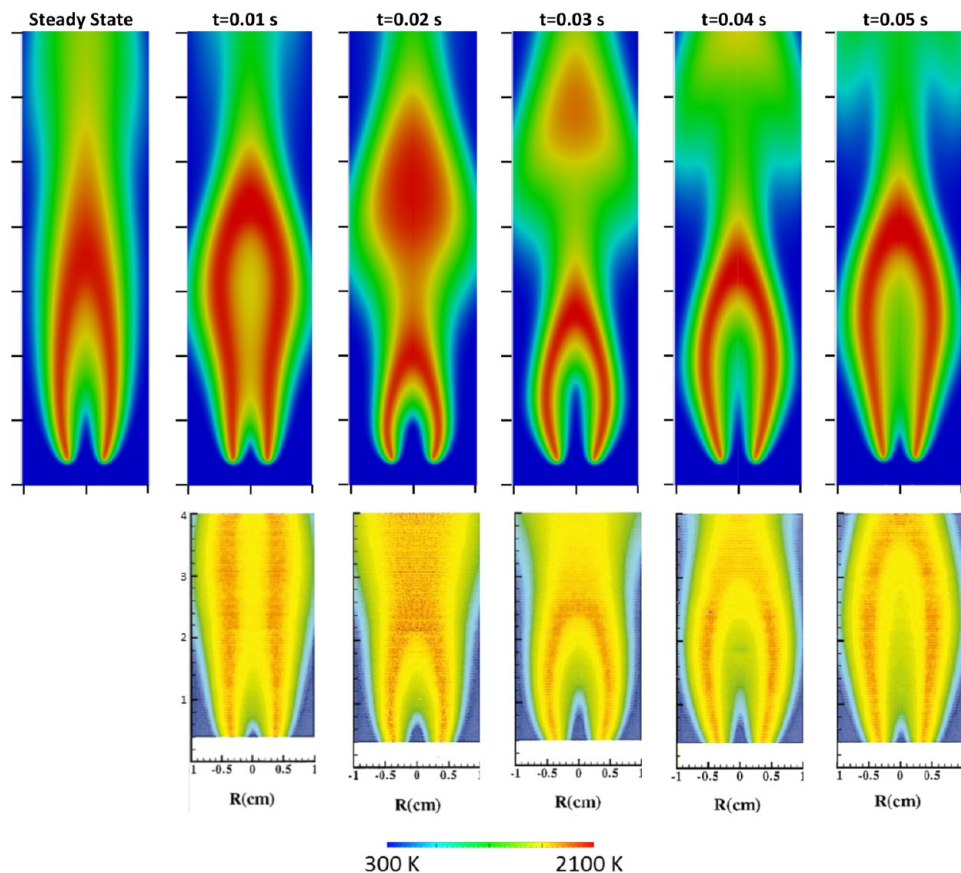


Figure 15. Transient CH_4/N_2 coflow diffusion flame: maps of temperature at several times. The calculated maps are reported in the first row, while the second row reports the measured maps.⁵⁹ The calculated maps cover a 20 mm \times 700 mm rectangular region. The distance between the ticks for each calculated map is equal to 1 cm. The times reported in the first row are measured starting from the fourth cycle of the flame.

though the adopted mesh in the axial direction was exactly the same, some small discrepancies between the 1D and 2D solutions can be observed. In particular, the 1D code predicts a smaller flame thickness and a lower maximum temperature (by about 10 K). As better discussed in ref 52, these differences are mainly associated with two-dimensional effects, which are obviously neglected in the 1D code (which is based on the similarity hypothesis). Moreover, while the 1D model solves the equations using a very accurate fully coupled method, laminarSMOKE introduces the unavoidable time-splitting error associated with the Strang algorithm.

Further numerical tests were performed in order to study the effects of the grid refinement on the steady-state solutions. For this purpose, in order to save computational time, the simulations were performed using a three-step global mechanism.⁵⁵ In particular, the tests were performed on structured meshes with equally spaced points, whose features are reported in Table 3. Figure 9 shows the calculated profiles of axial velocity and temperature along the axis for the different grids. It is quite evident that the differences between the second and third grids are negligible, which means that the solution can be considered grid-independent. It is important to remark that it is not possible to conclude that the solution with the POLIMI_C1C31212 detailed kinetic scheme (82 species) would be grid-independent for the same mesh because many intermediate species would be present over much smaller length scales compared with the length scales for species present in the three-step global mechanism results.

In order to further validate the code for the simulation of 3D cases, a fully 3D simulation of the counter-flow flame was performed by rotating the 2D mesh around the axis of symmetry of the system. Because of the symmetry of the system, the 2D and 3D solutions were expected to be the same. The comparison was performed on the coarsest grid, with 180 discretizations along the azimuthal direction, since for such a comparison a fine grid is not strictly necessary. Moreover, in order to save computational time, the three-step global mechanism was adopted. As a result, even though a fully 3D mesh was adopted, the computational time for performing the comparison was not prohibitive. As expected, the agreement between the two numerical simulations was very good, further demonstrating the reliability of the code: in particular, the relative error between the two solutions was always smaller than 10^{-6} .

4.3. $\text{CH}_4/\text{Air Coflow Flames (Steady-State)}$. The laminarSMOKE code was then used to simulate a series of six CH_4/air coflow flames that were experimentally and computationally studied by McEnally and Pfefferle⁵⁶ and Bennett et al.,⁵⁷ respectively. The problem geometry is specified in Figure 10. The inner jet flows from a circular tube (internal diameter of 11.1 mm). The outer jet's inner diameter is 95.2 mm, and the inner diameter of the cylindrical shield is 102 mm. Both the fuel and oxidizer streams are fed at ambient temperature and atmospheric pressure. The fuel is a mixture of CH_4 and air (called primary air) in different amounts. In particular, the CH_4 flow rate is the same for all six flames, while the primary air flow rate varies in such a way that the primary

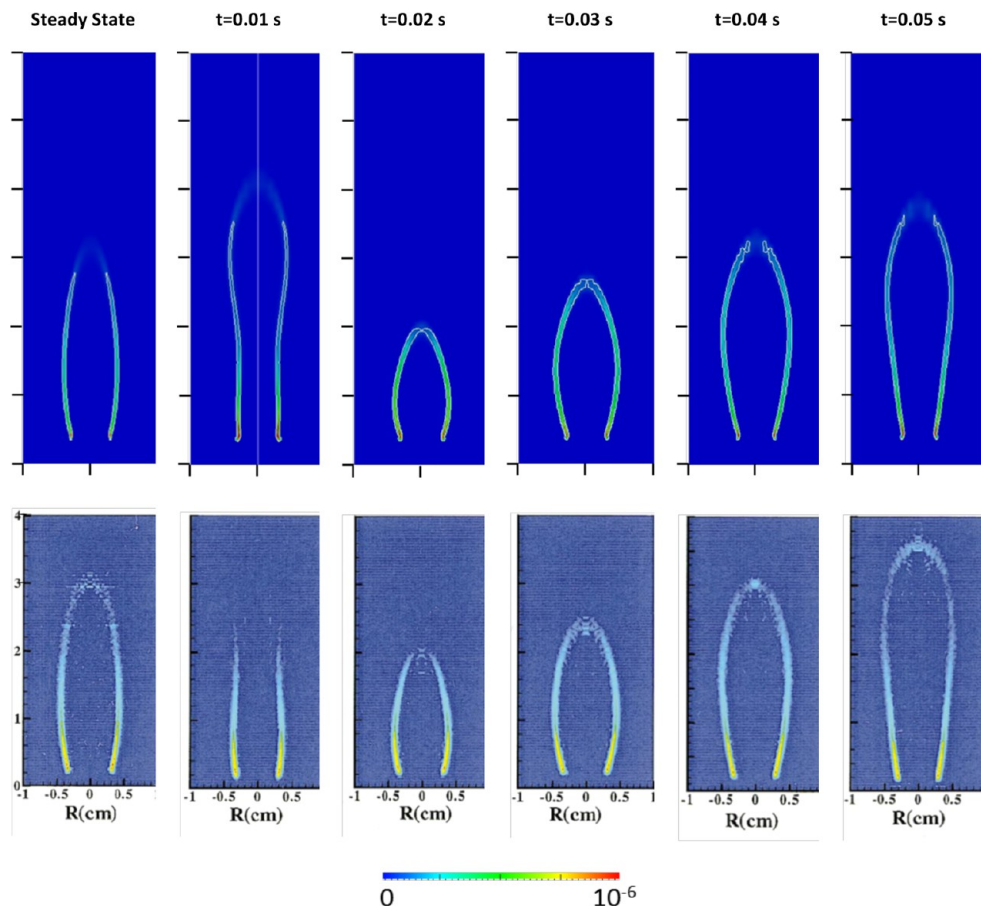


Figure 16. Transient CH_4/N_2 coflow diffusion flame: maps of CH mass fraction at several times. The calculated maps are reported in the first row, while the second row reports the measured maps.⁵⁹ The calculated maps cover a $20 \text{ mm} \times 700 \text{ mm}$ rectangular region. The distance between the ticks for each calculated map is equal to 1 cm. The times reported in the first row are measured starting from the fourth cycle of the flame.

equivalence ratio varies between ∞ and 2.5. The primary equivalence ratios, inlet flow rates, and inlet velocities are summarized in Table 4. The Reynolds number of the flames (evaluated with respect to the inner jet) is between ~ 38 and ~ 158 , corresponding to laminar conditions.

The simulations were carried out using a rectangular, non-equispaced, structured mesh of 9600 cells, with finest cells in the region immediately above the burner surface and minimum spacings of 0.25 and 0.2 mm along the axial and radial directions, respectively. Further refinements of the grid in the axial and radial directions did not result in any significant difference in the calculated solutions. The chemistry was modeled using the POLIMI HT1212 kinetic mechanism (198 species and 6307 reactions).⁴⁸

Table 5 reports the measured and calculated flame heights (i.e., the axial location where the maximum centerline temperature occurs) together with the peak temperatures along the axis. As expected, the flame height decreases (from 59 to 41 mm) with increasing premixing degree, while the peak temperature increases from 1960 to 2090 K. The agreement between the numerical predictions and the experimental data is satisfactory, although the calculated peak temperatures are always slightly lower than the experimental values.

Figure 11 presents the calculated maps of the temperature and the mass fractions of the main species for the flames with the largest ($\phi = \infty$) and smallest ($\phi = 2.5$) equivalence ratios. As the equivalence ratio decreases, the flame moves from a conventional non-premixed flame ($\phi = \infty$) to a flame having a

double flame structure ($\phi = 2.5$), that is, containing two different flame sheets: an inner rich, premixed flame and an external non-premixed flame where the rich products burn with the coflow air.⁵⁸

Figures 12 and 13 report the comparison between the experimental measurements⁵⁶ and the numerical predictions along the centerline for flames with $\phi = \infty$ and $\phi = 2.5$, respectively. The profiles are reported along a dimensionless coordinate defined as the ratio between the axial coordinate and the flame height. The overall agreement can be considered satisfactory. According to Bennett et al.,⁵⁷ the inflection points in the temperature profiles at $\phi = \infty$ are explained in terms of deposition of soot particles on the thermocouple. The only way to reproduce the inflection is not only to include a kinetic scheme accounting for soot formation but also a model for heat transfer to the thermocouple probe. The present simulation (which did not account for the heat transfer to the thermocouple probe) correctly predicts CH_4 , O_2 , and CO_2 but not H_2O , whose peak value is overestimated by $\sim 10\%$. Because of the low vapor pressure of H_2O at nonflame temperatures, the experimental measurements of H_2O presented serious difficulties in the calibration procedure. The experimental values reported in ref 57 were multiplied by a correction factor chosen to make the measured maximum concentration of H_2O agree with the maximum calculated value. For this reason, in our opinion it is more appropriate to look at the H_2O profiles only on a qualitative basis. The numerical model was able to correctly capture the peaks of

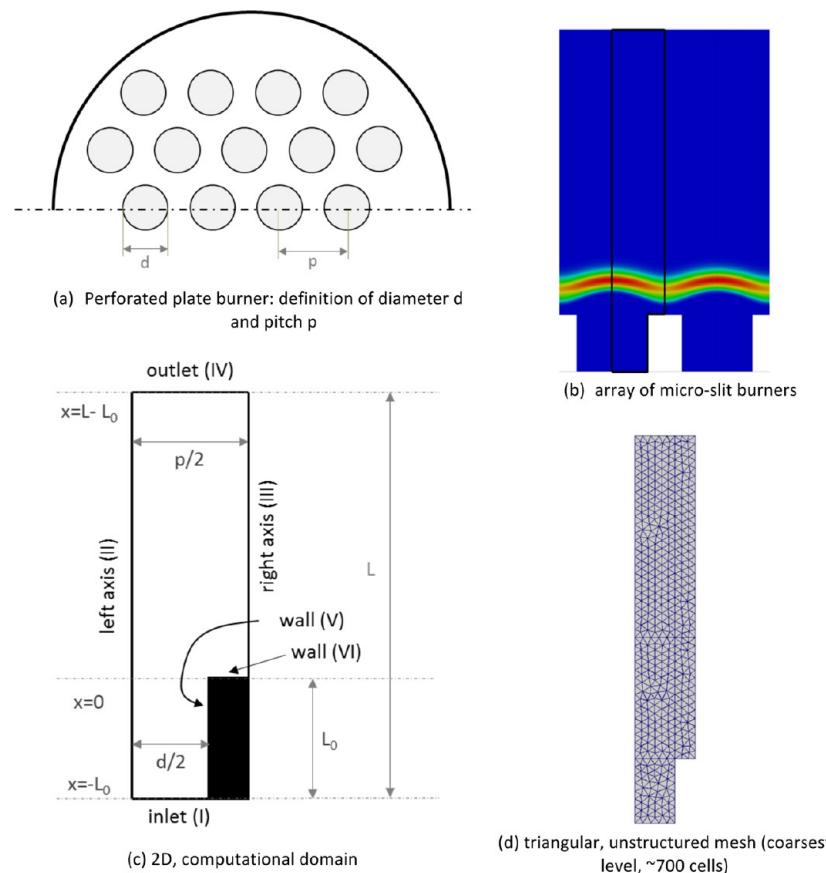


Figure 17. Perforated plate burner: details about the geometry, the computational domain, and the mesh.

C_3H_6 and OH , both in terms of positions and absolute values. The model overestimated the formation of C_6H_6 and C_{12}H_8 (reported in the Supporting Information), especially for the premixed flame. It should be noted that these two species are important soot precursors. Therefore, if the kinetic mechanism were to account for the formation of soot particles, the concentrations of C_6H_6 and C_{12}H_8 would be expected to decrease. Additional comparisons with the experimental data are reported in the Supporting Information, which provides a complete validation of the six flames with respect to all of the available experimental data.⁵⁶ In particular, a reasonable agreement with the experimental data was observed also for the profiles of ketene (CH_2CO) and propene (C_3H_6), especially considering that the experimental data for those species are accurate only within a factor of ~ 3 .

From the numerical results reported and discussed in this section, the reliability and accuracy of the proposed solver in the numerical modeling of the investigated coflow flames are quite evident.

4.4. Transient Methane/Air Diffusion Flame. The laminar SMOKE code was applied to a laminar diffusion flame under unsteady conditions, which was experimentally and numerically studied by Mohammed et al.⁵⁹ The fuel stream (65% CH_4 , 35% N_2 by volume) enters through a circular nozzle with an internal diameter of 4 mm and a thickness of 0.38 mm, while the coflow stream (21% O_2 , 79% N_2 by volume) enters through an annular region of internal diameter equal to 50 mm. Both streams are at 298 K and atmospheric pressure. The transient behavior was induced by a 20 Hz perturbation in the velocity profile of the fuel stream, according to the following expression:

$$\nu(r) = \nu_{\max} \left(1 - \frac{r^2}{R^2} \right) [1 + \epsilon \sin(2\pi ft)] \quad (18)$$

where ϵ and f are the amplitude and frequency of the perturbation, respectively, and ν_{\max} is equal to 70 cm/s. The coflow air is injected at 35 cm/s. The vertical sides of the chamber are bounded by a wall at 298 K, and the top is open to the atmospheric pressure. Experimental data are available for temperature and mole fractions of main species (CH_4 , O_2 , H_2O , CO_2 , CO , and H_2), minor species (C_2H_2 , C_6H_6 , and CH_2CO), and NO .

Following the work of Mohammed et al.,⁵⁹ we considered first the steady-state conditions (i.e., $f = 0$) and then the unsteady behavior for $\epsilon = 0.50$. In both cases, the calculations were performed using the POLIMI_C1C31212 kinetic scheme (82 species and 1485 reactions).⁴⁸ Because of the axisymmetry of the system, a 2D computational domain was chosen, with lengths of 51.2 and 102.4 mm in the radial and axial directions, respectively, as suggested in ref 22.

The steady-state calculations were performed on several structured meshes with increasing numbers of cells (up to 16 000) in both the axial and radial directions. The behavior of the solution with the mesh refinement was carefully studied by looking at the flame liftoff and the concentration of radical species such as OH , CH , and CH_2 . We found that a grid with 50 and 200 non-equispaced cells in the radial and axial directions, respectively, was fine enough to obtain a grid-independent solution. The corresponding minimum spacing along the axial and radial directions were 0.05 and 0.1 mm, respectively. The calculated flame liftoff (defined as the lowest

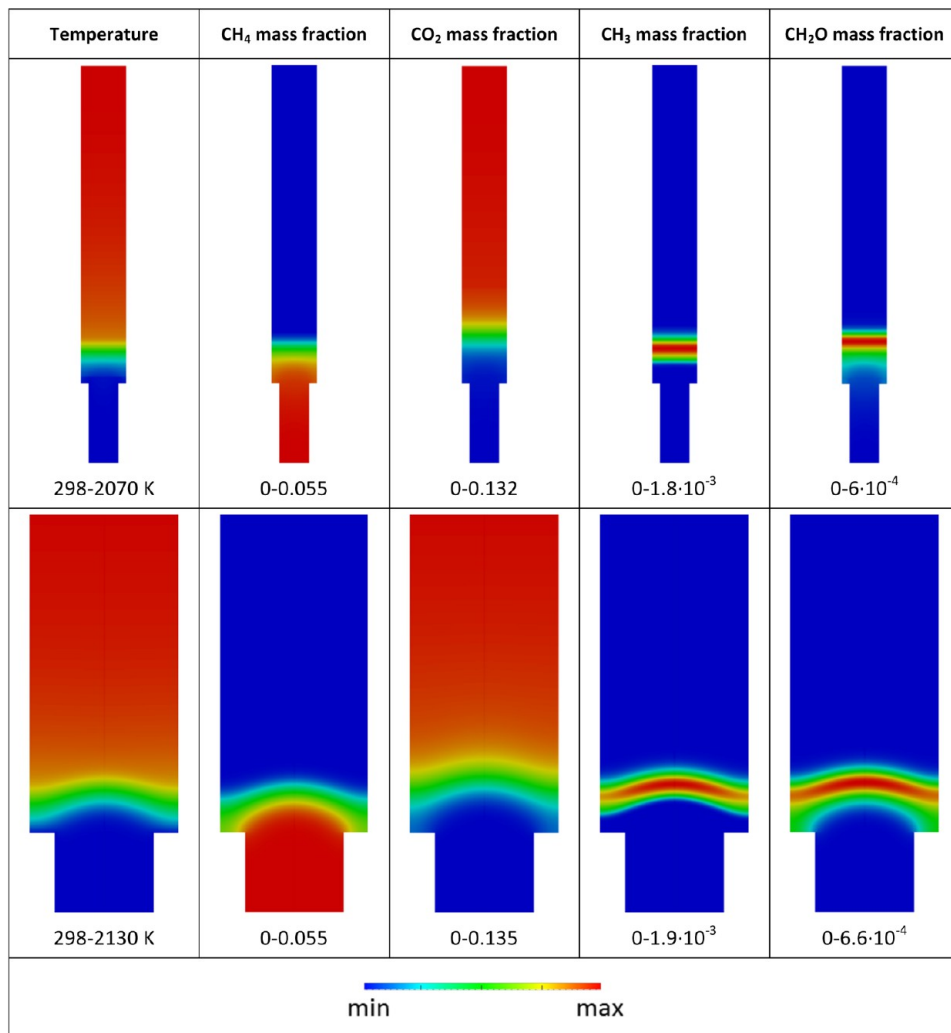


Figure 18. Calculated maps of temperature and mass fractions of selected species for the perforated plate burner. The maps in the first row refer to the case with $d = 0.03$ cm and those in the second row to the case with $d = 0.10$ cm. The numbers below each image are the minimum and maximum values of the plotted quantity.

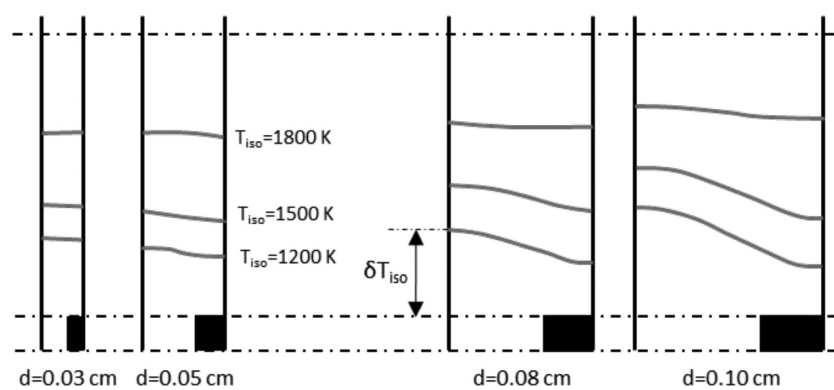


Figure 19. Definition of the δT_{iso} parameter (adapted from ref 62).

axial location where the flame reaches the temperature of 1000 K) was 4.5 mm for the finer mesh ($\sim 16\,000$ cells). Mohammed et al.⁵⁹ reported an experimental liftoff between 1.6 and 2.2 mm, but they obtained a computational liftoff of 6.6 mm using a kinetic scheme with 26 species and 83 reactions.⁶⁰ As reported in ref 5, these large differences can be explained on a kinetic basis, since the liftoff height is usually strongly dependent on the extinction strain rate of the mechanism.

The calculated maximum temperature was equal to 2070 K, in reasonable agreement with the thermocouple measurements of 2045 K. The peak temperature occurred at the radial location of ~ 3.75 mm. The flame heights (i.e., the axial locations where the maximum temperature occurs) were 34 and 36 mm for the thermocouple measurements and the calculations, respectively. Also in this case the agreement is quite satisfactory. The calculated maps of temperature and mass fractions of the major

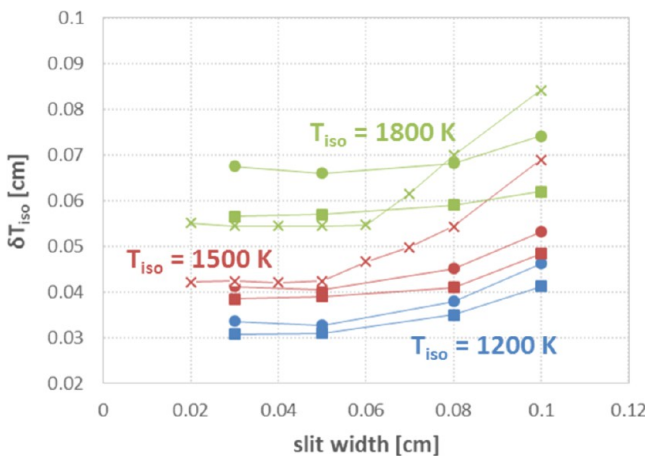


Figure 20. Calculated values of δT_{iso} (■) compared with the calculations performed by Bosch⁶¹ (×) and by Somers⁶² (●). Data from Bosch⁶¹ are available only for isothermal lines at 1500 and 1800 K.

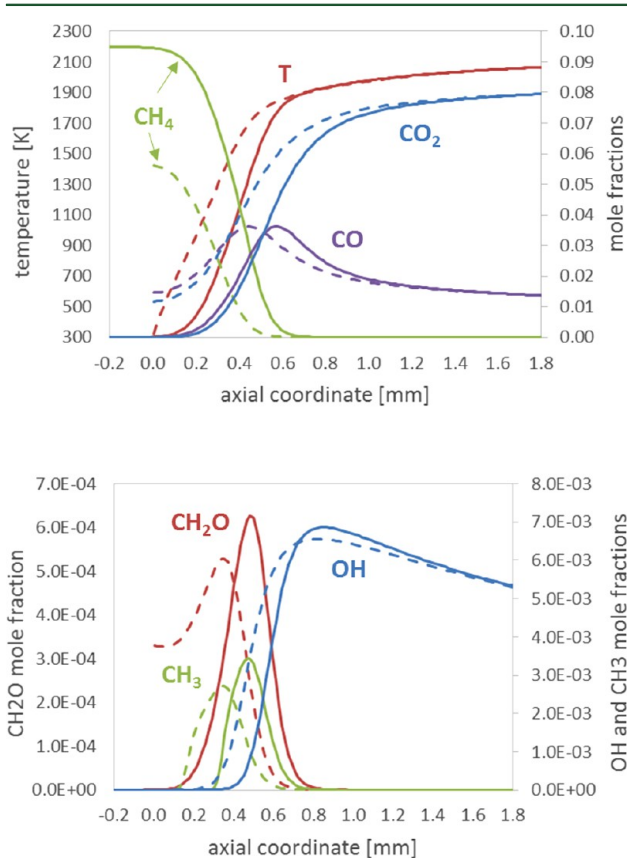


Figure 21. Perforated plate burner: temperature and mole fraction profiles of selected species along the left (II) boundary (solid lines) and the right (III) boundary (dashed lines).

species are reported in Figure 14. The typical features of non-premixed flames can be observed, with fuel (CH_4) inside the flame front and oxidizer (O_2) outside it, together with conversion to CO and H_2 and then to CO_2 and H_2O across the flame front. The model correctly captured the O_2 entrainment at the flame base and a slight outward-facing kink in the methane mole fraction at the liftoff height, as clearly evidenced by the experimental measurements.⁵⁹

The simulations of the unsteady conditions were performed on the finer mesh (~16 000 cells) by imposing a frequency of 20 Hz and an amplitude of 0.50. The typical time step adopted for the calculations was $\sim 2.5 \mu\text{s}$, corresponding to a maximum Courant number of 0.05. We assumed that three periods were sufficient to reach truly periodic behavior, which means that the data reported in the following refer to the fourth cycle. This decision was made by looking at the history of the temperature at three different fixed points along the central axis: no significant differences were registered between the third and fourth cycles. The simulations of the unsteady conditions were performed on 48 processors with a typical CPU time of ~ 2 s per time step.

Following the work of Day and Bell,²² we report in Figures 15 and 16 the time sequences of temperature and CH mass fraction, respectively, through one period of oscillation. The agreement of the shapes of the temperature and CH profiles with those observed experimentally by Mohammed et al.⁵⁹ is quite good. The transient behavior of the flame can also be better analyzed through the videos provided in the Supporting Information.

4.5. Perforated Plate Burner. A premixed laminar flame was also simulated using the laminarSMOKE code. In particular, we focused the attention on a perforated plate burner, as numerically studied by Bosch⁶¹ and Somers et al.^{62,63} The burner plate consists of drilled holes with diameter d and pitch p arranged in a honeycomb structure, as illustrated in Figure 17a. The main objective of the original works of Bosch⁶¹ and Somers et al.^{62,63} was to investigate the influence of the magnitude of the diameter d on the flame structure in order to determine whether such a burner can be well-characterized using one-dimensional models. Therefore, instead of a computationally expensive three-dimensional grid, because of symmetry considerations a two-dimensional model consisting of an array of microslit burners with width d and pitch p was adopted (Figure 17b). The 2D geometry used to model the slit burner flames is presented in Figure 17c along with details about the boundary conditions. At the inlet boundary (I) an isothermal fully developed parabolic velocity profile was prescribed, with mean velocity equal to 35 cm/s. The mole fraction composition of the inlet stream corresponds to a stoichiometric methane/air mixture (9.5% CH_4 , 19% O_2 , and 71.5% N_2 by volume). At the outlet (IV), a zero derivative normal to the boundary was prescribed. Symmetry conditions were imposed on the left (II) and right (III) boundaries. The burner's walls are cooled, and therefore, a fixed temperature of 298 K was imposed on boundaries (V) and (VI). For the simulation of the reactive flow field in the 2D geometry, the values for the width d , pitch p , domain length L , and inflow length L_0 had to be specified. Following the work of Somers,⁶² four different cases were investigated, with d equal to 0.03, 0.05, 0.08, and 0.1 cm. For all of these cases, the d/p ratio was kept fixed at 2/3, a quite common value for perforated plate burners. Too-small values for d/p can lead to early blowoff due to the high velocity in the slits, while a d/p value of 4/5 can be considered as an upper limit to avoid too large burner loads. The inflow length L_0 was set equal to 0.8 mm, and the domain length L was set to 4 mm. Later studies showed that these lengths are sufficiently large to obtain solutions that are not distorted by the outflow boundary. The simulations were performed using several unstructured, triangular meshes with increasing levels of detail, from ~ 700 cells (with a mean size equal to 0.01 mm) up to 10 000 cells (with a mean size of

Table 6. Analysis of the CPU Times for the Different Parts of the **laminarSMOKE** Code Using Results for the Counter-Flow Diffusion Flame Described in Section 4.2

kinetic scheme	ref	no. of species	no. of reactions	CPU time (s)			relative weights		
				reaction	transport prop.	transport	reaction	transport prop.	transport
DRM22	73	24	104	1.24	0.10	0.22	80.2%	6.3%	13.5%
POLIMI_Skeletal	48	25	155	1.24	0.09	0.21	79.2%	6.6%	14.2%
GRI12	11	32	177	2.42	0.15	0.32	83.5%	5.4%	11.1%
GRI21	11	49	279	4.91	0.33	0.61	83.8%	5.7%	10.5%
GRI30	11	53	325	5.98	0.38	0.71	84.4%	5.4%	10.2%
POLIMI_C1C31212	48	82	1460	18.75	0.942	1.49	88.5%	4.4%	7.1%
POLIMI_C1C31212NOx	48	113	1882	34.24	1.67	2.78	88.5%	4.4%	7.1%
POLIMI_HT1212	48	198	6247	146.8	4.84	7.55	92.2%	3.1%	4.7%

0.0025 mm). The latter was found to be sufficiently fine to have grid-independent solutions for all the cases under investigation. Figure 17d shows the coarser mesh adopted for the case corresponding to $d = 0.10$ cm. Of course, a rectangular, structured mesh would be a more appropriate choice because of the simplicity of the geometry under investigation. However, we opted for a triangular mesh in order to test the **laminarSMOKE** code also on unstructured grids. The simulations were carried out using the POLIMI C1C31212 kinetic scheme (82 species and 1485 reactions).⁴⁸

The main results under steady-state conditions are reported in Figure 18 for the cases corresponding to $d = 0.03$ cm and $d = 0.10$ cm. In particular, for each flame the 2D maps of temperature and mass fractions of the main species are shown. It is clear that the curvature of the isotherms increases in going from $d = 0.03$ cm to $d = 0.10$ cm: while for $d = 0.03$ cm the contours are almost straight lines, for $d = 0.1$ cm the temperature contours are clearly curved, indicating the departure from the flat-flame behavior. This effect can also be observed in the maps reporting the mass fraction of the CH₃ radical.

Bosch⁶¹ introduced an indicator to quantify the flatness of the flame (Figure 19). The so-called δT_{iso} parameter is defined as the distance of a certain isotherm with value T_{iso} above the burner at the left symmetry boundary (II). Obviously this height is equal to the height of the same isotherm above the burner at the right symmetry axis (III) if the flame is flat. If the flames becomes more curved, the height found at the left boundary will differ more and more from the one found at the right boundary. Figure 20 reports the calculated values of δT_{iso} for temperatures of 1200, 1500, and 1800 K together with calculations performed by Bosch⁶¹ (global one-step reaction) and Somers⁶² (skeletal kinetic mechanism with 15 species and 25 reactions). The results of the present work are quite similar to the calculations performed by Somers: the trend with respect to the slit width d is the same in both cases, but the results obtained in the present work are systematically lower than those of Somers.⁶² The simulations performed by Bosch⁶¹ show significant deviations from the present work and Somers' calculations, which could be due to the simplified, one-step global mechanism. Of course, further investigations are needed to confirm this point.

The detailed structure of the flame for $d = 0.10$ cm is shown in Figure 21, where the mass fraction profiles of the main species are reported along the left (II) and right (III) axes of symmetry. The two sets of profiles can be easily distinguished from each other. In particular, the temperature profile at the right side (III) is clearly shifted upstream with respect to the profile found at the center boundary (II). Although not shown

here, in contrast to the $d = 0.10$ cm results, for the $d = 0.03$ cm case the profiles already merge well before the reaction layer.

5. COMPUTATIONAL PERFORMANCE

In this section, the computational performance of the **laminarSMOKE** code is briefly described and discussed. In particular, attention is focused on the computational costs of the different parts of the code, the domain decomposition procedure adopted for distributing the calculations on parallel architectures, and the efficiency of the multiprocessor calculations.

5.1. CPU Times. As already discussed in section 3.1 and reported in Figure 1, the **laminarSMOKE** code is organized into three main parts: (i) the chemical step, in which the stiff ODE systems are integrated over the chosen time step; (ii) the evaluation of transport properties (mass diffusion coefficients, thermal conductivity, dynamic viscosity, and thermal diffusion coefficients); and (iii) the transport (convection and diffusion) step. The relative weights (in terms of CPU time) of these three parts are strongly affected by the complexity (number of species) of the kinetic mechanism adopted. Several tests were performed to measure these relative weights in order to optimize the code and better exploit parallel calculations. Only the results referring to the counter-flow diffusion flame studied in section 4.2 are summarized here.

The analysis was performed by using different kinetic schemes with different numbers of species ranging from 22 to 198. Table 6 reports the computational cost of the three parts in simulating a time interval of 10^{-5} s on a structured equispaced grid with 19 680 cells (mesh B in Table 3). As expected, the CPU times for all three phases increase with the number of species. The reaction step is the most consuming part of the code, independent of the kinetics, requiring more than 80–85% of the total computational time. The evaluation of the transport properties and the transport step cover 5–7% and 10% of the total time, respectively. Figure 22 better shows these trends: it can be observed that the CPU time of the reaction steps increases more than quadratically (~ 2.2) with respect to the number of species, while the transport properties increase with a power of ~ 1.8 and the transport step with a power of only ~ 1.7 . This means that increasing the number of species increases the relative weight of the reaction step, as is evident from Table 6. This has important consequences for adopting a parallelization strategy, as better explained in the next sections. Similar trends and results were also observed for the other flames (not reported here because of lack of space).

Since most of the computational time is spent in the reaction step, the numerical integration of the stiff ODE systems (eqs 14) requires a fast and robust ODE solver for very stiff problems. Several solvers with these features were tested: the DLSODE and DLSODA solvers belonging to the ODEPACK collection,⁶⁴ the DVODE⁶⁵ and CVODE⁶⁶ solvers, the RADAU5 integrator,⁶⁷ and the BzzOde class.⁶⁸ The best performance was obtained using the BzzOde solver,⁶⁸ a solver specifically conceived and optimized for solving very stiff ODE systems like those associated with reacting systems with detailed kinetics.⁶⁹ In particular, Table 7 reports the CPU times to solve a single ODE system in a computational cell when the detailed kinetic mechanism POLIMI_C1C31212 was adopted.

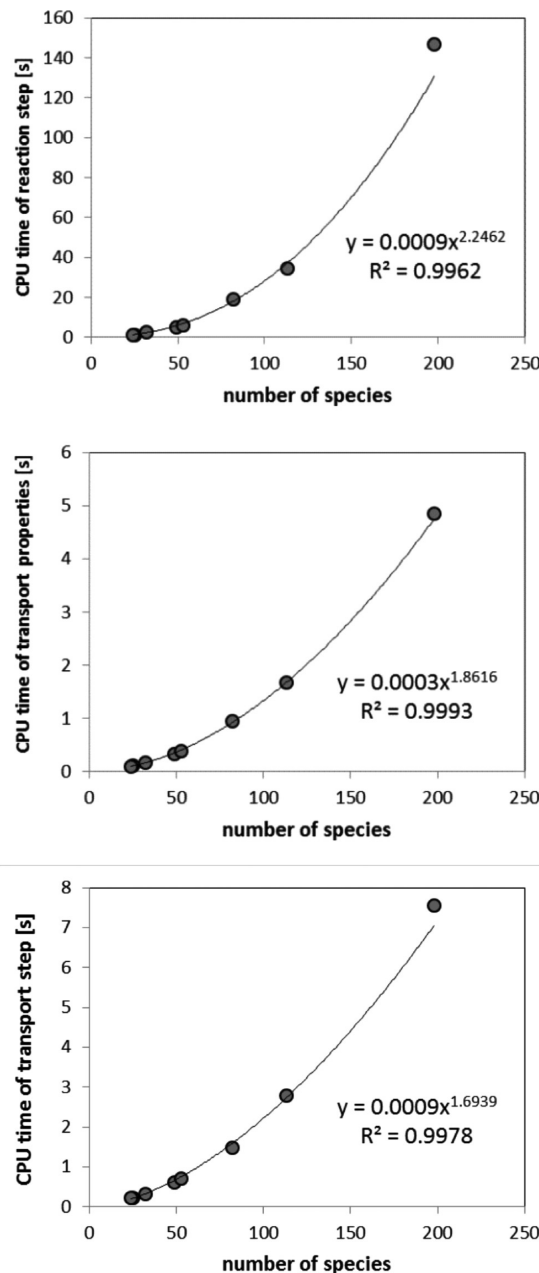


Figure 22. Analysis of the CPU times for the different phases of the laminarSMOKE code. The results refer to the counter-flow diffusion flame studied in section 4.2.

5.2. Domain Decomposition Procedure. Parallel calculations on distributed-memory machines are possible through the domain decomposition method (DDM). According to DDM, the mesh is split

into several submeshes, which are distributed over the processors available. The simulation then runs in parallel on the separate subdomains, and the communication between the processors occurs through the MPI protocol. The discretized governing equations are solved in each submesh with the appropriate boundary conditions (inner iteration). Once all submeshes have been calculated, relevant data about the interpolation boundaries is transferred among the different submeshes in an explicit manner (outer iteration). In this way, several submeshes can be solved simultaneously using different processors. The processors communicate only once per outer iteration. Thus, in general the amount of communication work is notably less than the amount of calculation work. One of the main advantages of this technique is its easy implementation and management, especially for very complex geometries. On the other hand, satisfactory computational efficiency can be achieved only if the mesh is correctly decomposed, that is, if the computational costs of the different submeshes are comparable. Several strategies can be implemented to improve the load balancing and reduce communication costs. In general, for homogeneous architectures (i.e., identical processors, as used in this work for all of the parallel computations), effective load balancing can be achieved by assigning to each processor a similar number of cells. For heterogeneous parallel machines, such as a network of workstations, a weighted distribution must be adopted to preferentially assign more cells to the faster processors and fewer cells to the slower processors.

For the combustion cases analyzed in the present work, in which large kinetic schemes were adopted, great attention must be devoted to the decomposition strategy. Unfortunately, when dealing with reacting problems, some regions of the computational domain can be significantly more involved in performing finite-rate chemical kinetics calculations during the reaction step. This is very evident from Figures 23 and 24, which report the CPU times required by each computational cell to perform the reaction step (i.e., to solve the local, stiff ODE system in eq 14) for the counter-flow diffusion flame studied in section 4.2 and the transient coflow flame analyzed in section 4.4, respectively. The CPU time required by the chemical step is not uniform, and as expected, it is usually larger in the region where the reactivity is higher, namely, in the core of the flame and on the flame front. To efficiently face such situations, it was necessary to design a domain decomposition procedure (based on the METIS libraries⁷⁰) that weighted the different cells according to their characteristic CPU times for solving the reaction step. The decomposition procedure was designed in order to assign to each processor a number of cells such that the sum of their weights is comparable to those for the other processors.

The characteristic weight of each cell corresponds to the CPU time spent by the code to solve the local ODE system (i.e., the chemical step) and is determined by advancing the solution over a single time step. Then, the decomposition procedure is performed using the numerical algorithms provided by the METIS libraries. In particular, the decomposition minimizes the number of cells along the boundaries of the subdomains in order to reduce the interdomain dependency, but at the same time it takes into account the weight assigned to each cell with the aim of balancing the computational load on each subdomain. In transient simulations, the decomposition procedure can be repeated in order to better follow the flame and keep a correct balance between

Table 7. List of the Different Stiff ODE Solvers for the Integration of the Chemical Step and the Corresponding CPU Times Required To Integrate the ODE System in Equation 14 over a Time Step of 10^{-5} s Using the POLIMI_C1C31212 Kinetic Mechanism

	ref	language	linear system solution	code available	license	CPU time (ms)
BzzOde	68	C++	direct	yes	free only for academic use	9
CVODE	66	C	direct/iterative	yes	free	12
DLSODA	65	FORTRAN	direct	yes	free	58
DLSODE	65	FORTRAN	direct	yes	free	40
DVODE	65	FORTRAN	direct	yes	free	11
RADAUS	67	FORTRAN	direct	yes	free	10.5

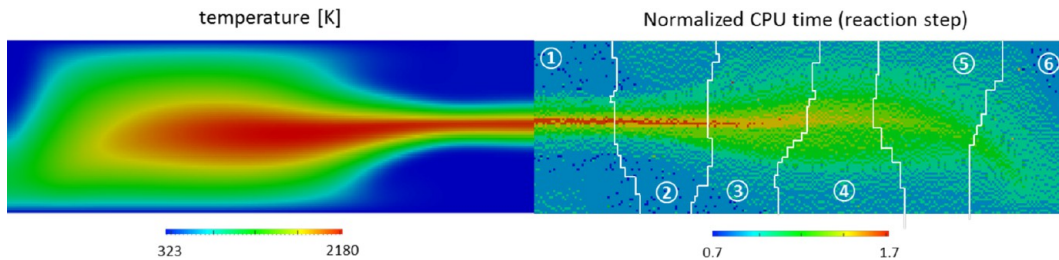


Figure 23. Counter-flow diffusion flame: maps of (left) temperature and (right) CPU time for integration of the chemical step in each computational cell. The CPU time is normalized to the mean CPU time evaluated with respect to all of the computational cells. On the right the weighted decomposition of the mesh into six submeshes is reported. The figure refers to a structured and equispaced computational mesh.

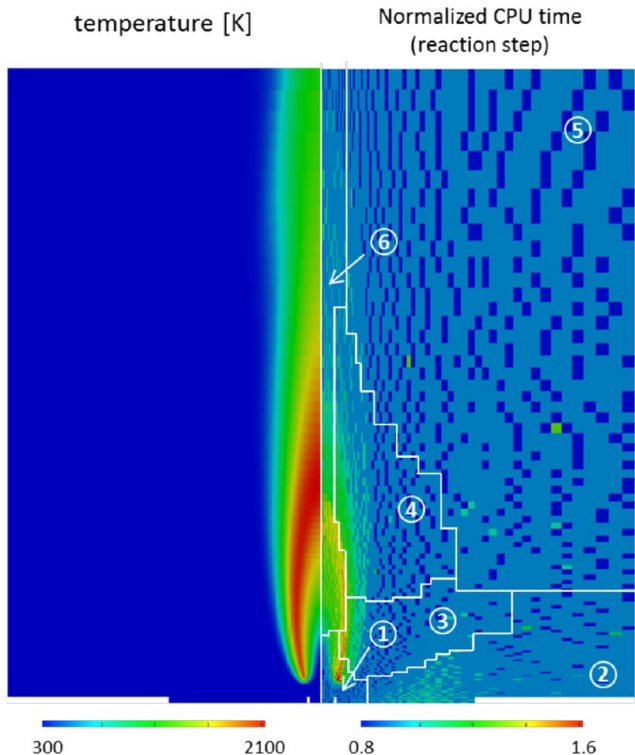


Figure 24. Transient CH_4/N_2 coflow diffusion flame: maps of (left) temperature and (right) CPU time for integration of the chemical step in each computational cell. The CPU time is normalized to the mean CPU time evaluated with respect to all of the computational cells. On the right the weighted decomposition of the mesh into six submeshes is reported. The figure refers to a structured and nonuniform computational mesh.

the subdomains, but this operation cannot be performed “on the fly” because it requires the simulation to be stopped.

As an example, the weighted decompositions for the two flames mentioned above are reported again in Figures 23 and 24 (only six processors are used for graphical reasons).

5.3. Parallel Performance. The parallel performance of the laminarSMOKE code was assessed for the counter-flow diffusion flame with a mesh consisting of 19 680 cells. The tests were performed on the same Infiniband platform described at the beginning of section 4, and the parallel performance was measured using up to 96 processors.

The scaling properties are measured by the parallel speed-up S_p and the efficiency η_p , which are defined as follows:

$$S_p = \frac{t_s}{t_p} \quad (19)$$

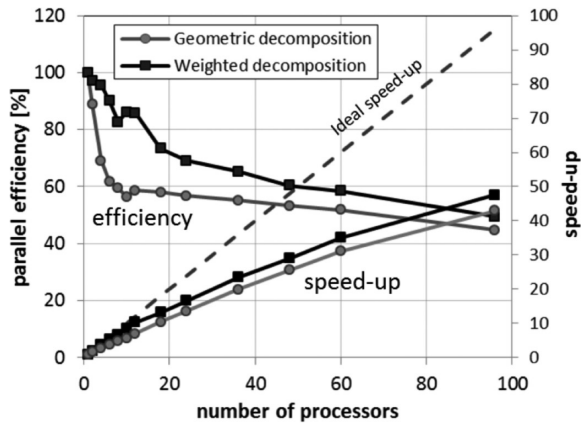


Figure 25. Parallel performance of the laminarSMOKE code. The results refer to the counter-flow diffusion flame simulated using the POLIMI_Skeletal kinetic scheme (25 species)⁴⁸ and a mesh with 19 680 cells.

Table 8. Numerical Simulation of Laminar and Turbulent Jet Flames: Parallel Performances of Several Solvers As Reported in the Literature

authors	ref.	species	cells	processors	efficiency
Ern et al. (1994)	74	16	4000 to 14000	16	60–70%
Bell et al. (2002)	23	65	122880	64	70–80%
Consul et al. (2003)	12	49	50000 to 180000	12	75–80%
Zhang et al. (2008)	75	51	16512	12	80%
Charest et al. (2010)	24	36	8064	384	70%
Tosatto et al. (2011)	9	16 to 222	7500 to 90000	16 to 128	70–90%
this work	25 to 198	19680	12 to 96	50–90%	

$$\eta_p = \frac{S_p}{p} \quad (20)$$

where t_s and t_p are the total wall times required to solve the problem with 1 and p processors, respectively. The integration of the chemical step (which requires most of the computational time) does not involve communication between the different subdomains, thus resulting in satisfactory parallel performances of the laminarSMOKE code. Figure 25 reports the speed-up and efficiency achieved by employing two different techniques to decompose the computational mesh among the processors: (i) a geometrical approach, in which the whole domain is decomposed by looking only at the geometry, such that each processor receives substantially the same number of cells; and (ii) the weighted approach (described in the previous section), in which each cell has a different weight proportional to the CPU time needed to integrate the ODE system corresponding to the chemical step (eq 14).

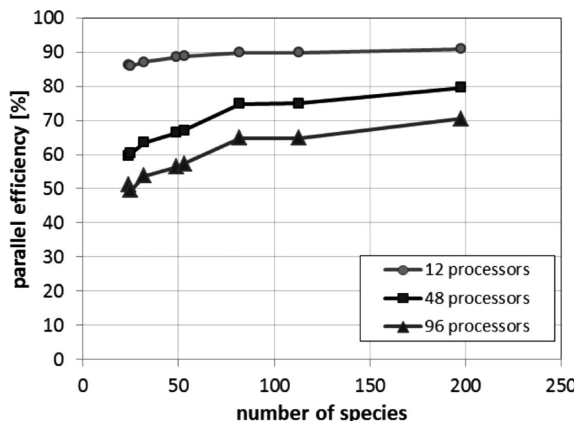


Figure 26. Parallel performances of the laminarSMOKE code. The results refer to the counter-flow diffusion flame on a mesh with 19 680 cells.

As expected, the efficiency decreases with the number of processors, but the overall performance can be considered satisfactory, especially considering the generality of the code and the possibility to work on arbitrarily complex meshes. In particular, it is quite evident that adopting the weighted decomposition results in a substantial improvement in the efficiency, especially when the number of processors is relatively small.

In Table 8 we have summarized the parallel performances of several codes used for the modeling of jet flames as reported in the literature. For each solver, the parallel efficiency (as defined in eq 20) is reported together with the number of species in the kinetic mechanism, the number of cells in the computational mesh, and the maximum number of processors adopted. Unfortunately, a direct comparison between the performance of laminarSMOKE and those of the different solvers is not straightforward because the collection of data summarized in Table 8 refers to a wide range of numbers of species (from 16 to 222) and numbers of processors (from 12 to 384). Moreover, the different solvers are also based on very different numerical techniques and were tested on different cluster architectures, which further complicates the comparison.

The impact of the kinetic mechanism on the parallel performance was investigated, and the results are summarized in Figure 26. The scaling performance improves as the number of species contained in the kinetic scheme increases. This result was also observed by Tosatto et al.,⁹ who clearly demonstrated that the size of the mechanism strongly affects the parallel efficiency by testing mechanisms containing 16 to 222 species. This result can be easily explained: by increasing the number of species, the role played by the transport step decreases, (i.e. the fraction of computational time devoted to the integration of the transport step becomes smaller). Since only the transport step requires interprocessor communication (because of the spatial operators in eq 12), this results in a benefit in terms of speed-up and parallel efficiency. This feature is very important because it allows the possibility to efficiently exploit the code for calculations with very detailed kinetic mechanisms.

6. CONCLUSIONS

In this paper we have described and analyzed laminarSMOKE, a new numerical platform for the simulation of laminar flames with detailed gas-phase chemistry that is built on top of the open-source OpenFOAM code. The platform is based on the operator-splitting approach and works on structured and unstructured meshes. It can be freely downloaded from the web (<http://www.opensmoke.polimi.it/>) and is open to external contributions.

The platform was applied to simulate several combustion systems with different degrees of complexity under both steady-

state and transient conditions. In particular, simulations with very detailed mechanisms (~200 species) in 2D were successfully performed. Good agreement with published experimental data for laminar coflow flames was achieved, and the proposed algorithm proved to be a robust, accurate solution method for laminar flames. The feasibility of the laminarSMOKE solver was further demonstrated by analyzing its performance on multiprocessor architectures. The code showed a reasonable scalability up to 96 processors (with parallel efficiency at least equal to 60%) for rectangular, structured meshes, which can be considered a good result, especially considering the generality of the code and the possibility to apply it to arbitrarily complex geometries. More interestingly, the observation by Tosatto et al.⁹ that the parallel scalability increases with the number of species in the adopted kinetic scheme was confirmed. This means that the laminarSMOKE code can be considered an ideal platform for the numerical simulation of combustion systems with very detailed kinetic schemes. Of course, it is important to remark that no definitive conclusions can be drawn about the performance of the code when unstructured or very irregular meshes are adopted.

The laminarSMOKE code was also extended to manage not only homogeneous reactions but also heterogeneous reactions on catalytic surfaces.⁷¹ Future developments should focus on improving the scalability and reducing the computational cost. In particular, the implementation of smart storage/retrieval methods⁷² for faster numerical integration of eq 14 should strongly improve the performance of the code. In addition, more accurate radiative heat transfer models are required in order to improve the predictive capabilities of the framework.

ASSOCIATED CONTENT

S Supporting Information

Additional comparisons with experimental data for the partially premixed coflow flames described in section 4.3 and videos referring to the ignition process of the counter-flow diffusion flame described in section 4.2 and the transient behavior of the CH₄/N₂ coflow flame described in section 4.4. This material is available free of charge via the Internet at <http://pubs.acs.org>.

AUTHOR INFORMATION

Corresponding Author

*Address: Department of Chemistry, Materials, and Chemical Engineering, Politecnico di Milano, P.zza Leonardo da Vinci 32, 20133 Milano, Italy. Phone: +39 02 2399 3283. Fax: +39 02 7063 8173. E-mail: alberto.cuoci@polimi.it.

Notes

The authors declare no competing financial interest.

REFERENCES

- (1) Gao, X.; Groth, C. P. A parallel solution—adaptive method for three-dimensional turbulent non-premixed combusting flows. *J. Comput. Phys.* **2010**, *229*, 3250–3275.
- (2) Law, C. K. *Combustion Physics*; Cambridge University Press: New York, 2006.
- (3) Ern, A.; Douglas, C. C.; Smooke, M. D. Detailed chemistry modeling of laminar diffusion flames on parallel computers. *Int. J. Supercomput.* **1995**, *9*, 167–186.
- (4) Smooke, M. D.; et al. Soot formation in laminar diffusion flames. *Combust. Flame* **2005**, *143*, 613–628.

- (5) Bennett, B. A. V.; Smooke, M. D. Local rectangular refinement with application to axisymmetric laminar flames. *Combust. Theory Modell.* **1998**, *2*, 221–258.
- (6) Bennett, B. A. V.; Smooke, M. D. Local rectangular refinement with application to nonreacting and reacting fluid flow problems. *J. Comput. Phys.* **1999**, *151*, 684–727.
- (7) Dworkin, S. B.; Bennett, B. A. V.; Smooke, M. D. A mass-conserving vorticity–velocity formulation with application to non-reacting and reacting flows. *J. Comput. Phys.* **2006**, *215*, 430–447.
- (8) Ern, A.; Smooke, M. D. Vorticity–Velocity Formulation for Three-Dimensional Steady Compressible Flows. *J. Comput. Phys.* **1993**, *105*, 58–71.
- (9) Tosatto, L.; Bennett, B. A. V.; Smooke, M. D. Parallelization strategies for an implicit Newton-based reactive flow solver. *Combust. Theory Modell.* **2011**, *15*, 455–486.
- (10) Knio, O. M.; Najm, H. N.; Wyckoff, P. S. A semi-implicit numerical scheme for reacting flow modeling. II: Stiff, operator split formulation. *J. Comput. Phys.* **1999**, *154*, 428–467.
- (11) Frenklach, M.; et al. http://www.me.berkeley.edu/gri_mech/.
- (12) Consul, R.; et al. Detailed numerical simulation of laminar flames by a parallel multiblock algorithm using loosely coupled computers. *Combust. Theory Modell.* **2003**, *7*, 525–544.
- (13) Becker, R.; Braack, M.; Rannacher, R. Numerical simulation of laminar flames at low Mach number with adaptive finite elements. *Combust. Theory Modell.* **1999**, *3*, 503–534.
- (14) D'Anna, A.; D'Alessio, A.; Kent, J. H. A computational study of hydrocarbon growth and the formation of aromatics in coflowing laminar diffusion flames. *Combust. Flame* **2001**, *125*, 1196–1206.
- (15) Liu, F.; et al. Effects of gas and soot radiation on soot formation in a coflow laminar ethylene diffusion flame. *J. Quant. Spectrosc. Radiat. Transfer* **2002**, *73*, 409–421.
- (16) Guo, H.; et al. The flame preheating effect on numerical modelling of soot formation in a two-dimensional laminar ethylene–air diffusion flame. *Combust. Theory Modell.* **2002**, *6*, 173–187.
- (17) Patankar, S. V. *Numerical Heat Transfer and Fluid Flow*; Taylor & Francis: London, 1980.
- (18) Roquemore, W. M.; Katta, V. R. Role of Flow Visualization in the Development of UNICORN. *J. Visualization* **2000**, *2*, 257–272.
- (19) Katta, V. R.; Roquemore, W. M. On the structure of a stretched/compressed laminar flamelet—Influence of preferential diffusion. *Combust. Flame* **1995**, *100*, 61–70.
- (20) Katta, V. R.; Goss, L. P.; Roquemore, W. M. Numerical investigations of transitional H₂/N₂ jet diffusion flames. *AIAA J.* **1994**, *32*, 84–94.
- (21) Burman, E.; Ern, A.; Giovangigli, V. Bunsen Flames Simulation by Finite Elements on Adaptively Refined Unstructured Triangulations. *Combust. Theory Modell.* **2004**, *8*, 65–84.
- (22) Day, M. S.; Bell, J. B. Numerical simulation of laminar reacting flows with complex chemistry. *Combust. Theory Modell.* **2000**, *4*, 535–556.
- (23) Bell, J. B.; et al. A parallel adaptive projection method for low Mach number flows. *Int. J. Numer. Methods Fluids* **2002**, *40*, 209–216.
- (24) Charest, M. R. J.; Groth, C. P. T.; Gulder, O. L. A computational framework for predicting laminar reactive flows with soot formation. *Combust. Theory Modell.* **2010**, *14*, 793–825.
- (25) Dobbins, R. R.; Smooke, M. D. A Fully Implicit, Compact Finite Difference Method for the Numerical Solution of Unsteady Laminar Flames. *Flow, Turbul. Combust.* **2010**, *85*, 763–799.
- (26) Cuoci, A.; et al. A computational tool for the detailed kinetic modeling of laminar flames: Application to C₂H₄/CH₄ coflow flames. *Combust. Flame* **2013**, *160*, 870–886.
- (27) OpenFOAM. www.openfoam.org, 2011.
- (28) Chapman, S.; Cowling, T. G. *The Mathematical Theory of Non-Uniform Gases*; Cambridge University Press: Cambridge, U.K., 1970.
- (29) Curtiss, C. F.; Hirschfelder, J. O. Transport properties of multicomponent gas mixtures. *J. Chem. Phys.* **1949**, *17*, 550–555.
- (30) Smooke, M. D.; Mitchell, R. E.; Keyes, D. E. Numerical solution of two-dimensional axisymmetric laminar diffusion flames. *Combust. Sci. Technol.* **1989**, *67*, 85–122.
- (31) Coffee, T. P.; Heimerl, J. M. Transport algorithms for premixed laminar steady-state flames. *Combust. Flame* **1981**, *43*, 273–289.
- (32) Dixon-Lewis, G. Flame Structure and Flame Reaction Kinetics. II. Transport Phenomena in Multicomponent Systems. *Proc. R. Soc.* **1968**, *307*, 111–135.
- (33) Ern, A.; Giovangigli, V. Thermal Diffusion Effects in Hydrogen–Air and Methane–Air Flames. *Combust. Theory Modell.* **1998**, *2*, 349–372.
- (34) Dworkin, S. B.; Smooke, M. D.; Giovangigli, V. The impact of detailed multicomponent transport and thermal diffusion effects on soot formation in ethylene/air flames. *Proc. Combust. Inst.* **2009**, *32*, 1165–1172.
- (35) Hall, R. J. The radiative source term for plane-parallel layers of reacting combustion gases. *J. Quant. Spectrosc. Radiat. Transfer* **1993**, *49*, 517–523.
- (36) Kee, R. J.; Miller, J. A. A split-operator, finite-difference solution for axisymmetric laminar-jet diffusion flames. *AIAA J.* **1978**, *16*, 169–176.
- (37) Oran, E. S.; Boris, J. P. *Numerical Simulation of Reactive Flow*; Cambridge University Press: Cambridge, U.K., 2001.
- (38) Duarte, M.; et al. New resolution strategy for multi-scale reaction waves using time operator splitting, space adaptive multi-resolution and dedicated high order implicit/explicit time integrators. *SIAM J. Sci. Comput.* **2012**, *34*, 76–104.
- (39) Nonaka, A.; et al. A deferred correction coupling strategy for low Mach number flow with complex chemistry. *Combust. Theory Modell.* **2012**, *16*, 1053–1088.
- (40) Ropp, D. L.; Shadid, J. N.; Ober, C. C. Studies of the accuracy of time integration methods for reaction–diffusion equations. *J. Comput. Phys.* **2004**, *194*, 544–574.
- (41) Ropp, D. L.; Shadid, J. N. Stability of operator splitting methods for systems with indefinite operators: Advection–diffusion–reaction systems. *J. Comput. Phys.* **2009**, *228*, 3508–3516.
- (42) Ren, Z.; Pope, S. B. Second-order splitting schemes for a class of reactive systems. *J. Comput. Phys.* **2008**, *227*, 8165–8176.
- (43) Sportisse, B. An analysis of operator splitting techniques in the stiff case. *J. Comput. Phys.* **2000**, *161*, 140–168.
- (44) Strang, G. On the construction and comparison of difference schemes. *SIAM J. Numer. Anal.* **1968**, *5*, 506–517.
- (45) Saad, Y. *Iterative Methods for Sparse Linear Systems*, 2nd ed.; Society for Industrial and Applied Mathematics: Philadelphia, 2003.
- (46) Issa, R. I. Solution of the Implicitly Discretized Fluid Flow Equation by Operator Splitting. *J. Comput. Phys.* **1986**, *62*, 40–65.
- (47) Ranzi, E.; et al. Wide-range kinetic modeling study of the pyrolysis, partial oxidation, and combustion of heavy *n*-alkanes. *Ind. Eng. Chem. Res.* **2005**, *44*, 5170–5183.
- (48) Ranzi, E.; et al. Hierarchical and comparative kinetic modeling of laminar flame speeds of hydrocarbon and oxygenated fuels. *Prog. Energy Combust. Sci.* **2012**, *38*, 468–501.
- (49) Cuoci, A.; et al. Formation of soot and nitrogen oxides in unsteady counterflow diffusion flames. *Combust. Flame* **2009**, *156*, 2010–2022.
- (50) Frassoldati, A.; Faravelli, T.; Ranzi, E. The ignition, combustion and flame structure of carbon monoxide/hydrogen mixtures. Note 1: Detailed kinetic modeling of syngas combustion also in presence of nitrogen compounds. *Int. J. Hydrogen Energy* **2007**, *32*, 3471–3485.
- (51) Roache, P. J. Perspective: A method for uniform reporting of grid refinement studies. *J. Fluids Eng.* **1994**, *116*, 404–413.
- (52) Amantini, G.; et al. Computational and experimental study of steady axisymmetric non-premixed methane counterflow flames. *Combust. Theory Modell.* **2007**, *11*, 47–72.
- (53) Chaniotis, A. K.; et al. Remeshed smoothed particle hydrodynamics for the simulation of laminar chemically reactive flows. *J. Comput. Phys.* **2003**, *191*, 1–17.
- (54) Lutz, A. E.; et al. OPPDIF: A Fortran program for computing opposed-flow diffusion flames; Sandia Report SAND96-8243; Sandia National Laboratories: Livermore, CA, 1997.
- (55) Westbrook, C. K.; Dryer, F. L. Chemical kinetic modeling of hydrocarbon combustion. *Prog. Energy Combust. Sci.* **1984**, *10*, 1–57.

- (56) McEnally, C. S.; Pfefferle, L. D. Experimental study of nonfuel hydrocarbon concentrations in coflowing partially premixed methane & air flames. *Combust. Flame* **1999**, *118*, 619–632.
- (57) Bennett, B. A. V.; et al. Computational and experimental study of axisymmetric coflow partially premixed methane/air flames. *Combust. Flame* **2000**, *123*, 522–546.
- (58) Yamaoka, I.; Tsuji, H. The structure of rich fuel-air flames in the forward stagnation region of a porous cylinder. *Fifteenth Symposium (International) on Combustion* **1974**, *15*, 637–644.
- (59) Mohammed, R. H.; et al. *Computational and experimental study of a forced, time-varying, axisymmetric, laminar diffusion flame*. *Proceedings of the Combustion Institute* **1998**, *27*, 693–702.
- (60) Smooke, M. D.; et al. Computational and experimental study of OH and CH radicals in axisymmetric laminar diffusion flames. *Symp. (Int.) Combust.* **1992**, *24*, 813–821.
- (61) Bosch, W. M. M. L. *Two-Dimensional Modelling of Flat Flames*; EUT Internal Report, Faculty of Mechanical Engineering, Eindhoven University of Technology: Eindhoven, The Netherlands, 1993.
- (62) Somers, L. M. T. The Simulation of Flat Flames with Detailed and Reduced Chemical Models. Ph.D. Thesis, Eindhoven University of Technology, Eindhoven, The Netherlands, 1994.
- (63) Somers, L. M. T.; De Goey, L. P. H. A numerical study of a premixed flame on a slit burner. *Combust. Sci. Technol.* **1995**, *108*, 121–132.
- (64) Hindmarsh, A. C., ODEPACK: A Systematized Collection of ODE Solvers. In *Scientific Computing*; Stepleman, R. S., Ed.; North-Holland: Amsterdam, 1983; pp 55–64.
- (65) Brown, P. N.; Byrne, G. D.; Hindmarsh, A. C. VODE: A Variable Coefficient ODE Solver. *SIAM J. Sci. Stat. Comput.* **1989**, *10*, 1038–1051.
- (66) Cohen, S. D.; Hindmarsh, A. C. CVODE: A Stiff/Nonstiff ODE Solver in C. *Comput. Phys.* **1996**, *10*, 138–143.
- (67) Hairer, E.; Wanner, G. *Solving Ordinary Differential Equations: Stiff and Differential-Algebraic Problems*, 2nd ed.; Springer Series in Computational Mathematics; Vol. 14; Springer: Berlin, 1996.
- (68) Buzzi-Ferraris, G.; Manca, D. BzzOde: A new C++ class for the solution of stiff and non-stiff ordinary differential equation systems. *Comput. Chem. Eng.* **1998**, *22*, 1595–1621.
- (69) Manca, D.; et al. Numerical modeling of oxidation and combustion processes. *Combust. Theory Modell.* **2001**, *5*, 185–199.
- (70) Karypis, G.; Kumar, V. METIS: *Unstructured Graph Partitioning and Sparse Matrix Ordering System*, version 4.0, 2009; <http://glaros.dtc.umn.edu/gkhome/metis/metis/overview>.
- (71) Maestri, M.; Cuoci, A. Coupling CFD with detailed microkinetic modeling in heterogeneous catalysis. *Chem. Eng. Sci.* **2013**, *96*, 106–117.
- (72) Pope, S. B. Computationally efficient implementation of combustion chemistry using in-situ adaptive tabulation. *Combust. Theory Modell.* **1997**, *1*, 41–63.
- (73) Kazakov, A.; Frenklach, M. <http://www.me.berkeley.edu/drm/>.
- (74) Ern, A.; Douglas, C. C.; Smooke, M. D. Detailed Chemistry Modeling of Laminar Diffusion Flames on Parallel Computers. *Int. J. Supercomput. Appl. High Perform. Comput.* **1994**, *9*, 167–186.
- (75) Zhang, Q.; Guo, H.; Liu, F.; Smallwood, G. J.; Thomson, M. J. Implementation of an advanced fixed sectional aerosol dynamics model with soot aggregate formation in a laminar methane/air coflow diffusion flame. *Combust. Theory Modell.* **2008**, *12*, 621–641.